Department of Applied Physics

Vacancy-type defects in Si, Ge and SiGe studied with positron annihilation spectroscopy

Simo Kilpeläinen

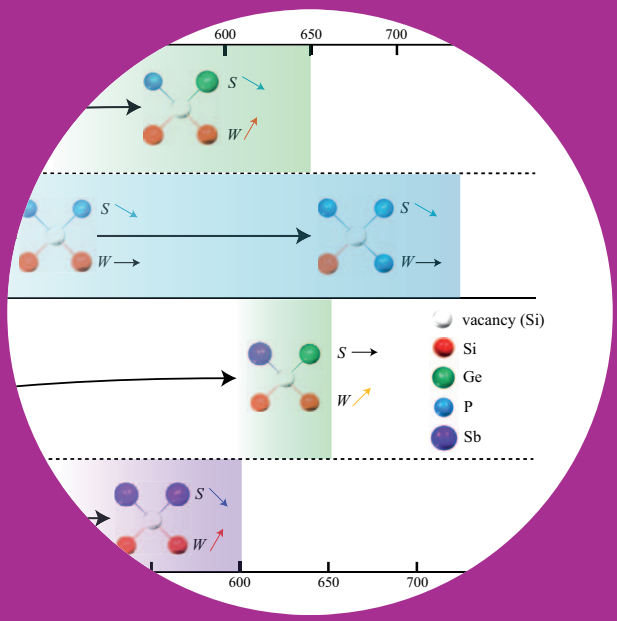

Aalto University

DOCTORAL DISSERTATIONS

Aalto University publication series
DOCTORAL DISSERTATIONS 64/2011

Vacancy-type defects in Si, Ge and SiGe studied with positron annihilation spectroscopy

Simo Kilpeläinen

Doctoral dissertation for the degree of Doctor of Science in Technology to be presented with due permission of the School of Science for public examination and debate in Auditorium G at the Aalto University School of Science (Espoo, Finland) on the 9th of September 2011 at 13 o'clock.

Aalto University
School of Science
Department of Applied Physics

Supervisor
Prof. Martti Puska

Instructor
Doc. Filip Tuomisto, PhD

Preliminary examiners
Prof. Matti Alatalo, Lappeenranta University of Technology, Finland
Prof. Mircea Guina, Tampere University of Technology, Finland

Opponent
Prof. Hartmut Bracht, University of Münster, Germany

Aalto University publication series
DOCTORAL DISSERTATIONS 64/2011

© Simo Kilpeläinen

ISBN 978-952-60-4229-9 (pdf)
ISBN 978-952-60-4228-2 (printed)
ISSN-L 1799-4934
ISSN 1799-4942 (pdf)
ISSN 1799-4934 (printed)

Aalto Print
Helsinki 2011

Finland

The dissertation can be read at http://lib.tkk.fi/Diss/

Aalto University

Abstract

Aalto University, P.O. Box 11000, FI-00076 Aalto www.aalto.fi

Author
Simo Kilpeläinen

Name of the doctoral dissertation
Vacancy-type defects in Si, Ge and SiGe studied with positron annihilation spectroscopy

Publisher School of Science

Unit Department of Applied Physics

Series Aalto University publication series DOCTORAL DISSERTATIONS 64/2011

Field of research Experimental physics

Manuscript submitted 14 June 2011 **Manuscript revised** 19 August 2011

Date of the defence 9 September 2011 **Language** English

☐ **Monograph** ☒ **Article dissertation (summary + original articles)**

Abstract

Electrical (and sometimes also mechanical) properties of a semiconductor are greatly influenced by various kinds of defects present in the material. Point defects such as vacancies and vacancy-impurity complexes are very common and can be introduced into the material both during growth and device fabrication. Positron annihilation spectroscopy is a useful tool for detecting and studying these types of defects. In this work, vacancy-type defects are studied and their properties examined in silicon, silicon-germanium and germanium.

Vacancy-donor complexes are one of the fundamental defects behind the electrical deactivation of n-type dopants in Si and SiGe. In this work, the vacancy-donor pair also known as the E center is studied in phosphorus- and antimony-doped SiGe. The annealing of the V-P (vacancy-phosphorus) pair in strained SiGe with different Ge contents is investigated with the help of an Arrhenius-like kinetic model and dissociation energies around 1 eV are obtained for the defect. Accumulation of germanium atoms around the defect during annealing is observed. The evolution of the V-Sb pair during annealing is studied in Si0.8Ge0.2 with different dopant concentrations. Ge accumulation around the defects is observed also in these samples. Small Ge clusters are detected in the samples after the annealing.

Deliberate introduction of defects by irradiation and ion implantation are common procedures for defect studies. In this work, proton-irradiated Ge is studied with an in situ annealing experiment. Two annealing stages are observed at 100 K and 200 K. The first stage is attributed to the Frenkel pair and the second to the monovacancy. Divacancy formation is observed following the second annealing stage, and these divacancies are found to be stable at room temperature. Helium co-implantation as a means to control boron diffusion profiles in B-implanted Si is studied. Nanovoids able to trap interstitials formed during B implantation are observed after the He implantation.

Novel solar cell materials consisting of Si nanocrystals embedded within an SiO2 matrix are studied in this work. The nanocrystals are formed by annealing Si/SiO2 multilayers at 1100C in N2. Interfaces between the nanocrystals and the SiO2 matrix are probed with positrons and photoluminescence. Nanocrystal formation is found to be optimized in samples with 2 nm thick Si layers.

Keywords Positrons, defects, semiconductors, silicon, germanium, E centers, vacancies

ISBN (printed) 978-952-60-4228-2 **ISBN (pdf)** 978-952-60-4229-9

ISSN-L 1799-4934 **ISSN (printed)** 1799-4934 **ISSN (pdf)** 1799-4942

Location of publisher Espoo **Location of printing** Helsinki **Year** 2011

Pages 113 **The dissertation can be read at** http://lib.tkk.fi/Diss/

Aalto-yliopisto

Tiivistelmä

Aalto-yliopisto, PL 11000, 00076 Aalto www.aalto.fi

Tekijä
Simo Kilpeläinen

Väitöskirjan nimi
Piissä, germaniumissa ja piigermaniumissa olevien vakanssityyppisten virheiden tutkiminen positroniannihilaatiospektroskopialla

Julkaisija Perustieteiden korkeakoulu

Yksikkö Teknillisen fysiikan laitos

Sarja Aalto University publication series DOCTORAL DISSERTATIONS 64/2011

Tutkimusala Kokeellinen fysiikka

Käsikirjoituksen pvm 14.06.2011 **Korjatun käsikirjoituksen pvm** 19.08.2011

Väitöspäivä 09.09.2011 **Kieli** Englanti

☐ **Monografia** ☒ **Yhdistelmäväitöskirja (yhteenveto-osa + erillisartikkelit)**

Tiivistelmä

Useat erityyppiset virheet vaikuttavat merkittävästi puolijohteiden sähköisiin (ja joskus myös mekaanisiin) ominaisuuksiin. Pistevirheet kuten vakanssit ja vakanssi-epäpuhtauskompleksit ovat hyvin yleisiä ja niitä syntyy materiaaleihin kasvatuksen ja prosessoinnin aikana. Positroniannihilaatiospektroskopia on käytännöllinen väline tällaisten virheiden havainnointiin ja tutkimiseen. Tässä työssä on tutkittu vakanssityyppisiä virheitä ja niiden ominaisuuksia piissä, piigermaniumissa sekä germaniumissa.

Vakanssi-donorikompleksit ovat eräitä tyypillisimmistä n-tyypin seostusatomien sähköistä deaktivaatiota aiheuttavista virheistä piissä ja piigermaniumissa. Tässä työssä on tutkittu vakanssi-donoripareja eli E-keskuksia fosfori- ja antimoniseostetussa piigermaniumissa. Vakanssi-fosforiparin toipumista piigermaniumissa (Ge-osuus 10-30%) on tutkittu Arrhenius-tyyppisen ensimmäisen kertaluvun kineettisen mallin avulla ja saatu virheen dissosiaatioenergiaksi n. 1 eV. Germaniumin kerääntymistä virheiden ympärille on todettu toivutuksen aikana. Vakanssi-antimoniparin kehittymistä toivutuskokeen aikana on tutkittu piigermaniumissa (Ge-osuus 20%). Germaniumin kerääntymistä virheiden läheisyyteen on todettu myös näissä näytteissä. Pieniä germaniumklustereita on havaittu toivotuksen jälkeen.

Virheiden tarkoituksellinen synnyttäminen näytteisiin säteilytyksen tai ioni-istutuksen keinoin on tyypillistä virhetutkimuksessa. Tässä työssä protonisäteilytettyä germaniumia on tutkittu in situ -toivutuskokeella. Kaksi toipumisvaihetta on havaittu 100 K:n ja 200 K:n tienoilla. Ensimmäinen vaihe on yhdistetty Frenkel-parien ja toinen monovakanssien toipumiseen. Toisen toipumisvaiheen jälkeen on havaittu näytteessä divakanssien muodostumista, ja niiden on todettu olevan vakaita huoneenlämpötilassa. Heliumin oheisistutusta on tutkittu keinona säädellä boorin diffuusiota boori-istutetussa piissä. B-istutuksen aikana syntyviä välisija-atomeja loukkuunnuttamaan kykeneviä nanoaukkoja on havaittu muodostuvan He-istutuksessa.

Uudenlaisia piidioksidiin upotetuista piinanokiteistä koostuvia aurinkokennomateriaaleja on tutkittu tässä työssä. Nanokiteet on synnytetty toivuttamalla pii/piidioksidimonikerroksista koostuvaa näytettä 1100-asteisessa typpikaasussa. Nanokiteiden ja piidioksidin välisiä rajapintoja on tutkittu positronien ja fotoluminesenssin avulla. Nanokiteiden muodostumisen on todettu olevan optimaalista näytteissä, joissa piikerros on 2 nm paksu.

Avainsanat Positronit, hilavirheet, puolijohteet, pii, germanium, E-keskukset, vakanssit

ISBN (painettu) 978-952-60-4228-2 **ISBN (pdf)** 978-952-60-4229-9

ISSN-L 1799-4934 **ISSN (painettu)** 1799-4934 **ISSN (pdf)** 1799-4942

Julkaisupaikka Espoo **Painopaikka** Helsinki **Vuosi** 2011

Sivumäärä 113 **Luettavissa verkossa osoitteessa** http://lib.tkk.fi/Diss/

Preface

The work presented in this thesis was conducted in the positron group in the Department of Applied Physics at the Aalto University School of Science between September 2007 and June 2011.

I wish to thank my instructor, Doc. Filip Tuomisto, for all the help and advice he has provided during these years, and furthermost for giving me an opportunity to work and complete this thesis in the group. I thank Doc. Jonatan Slotte for being almost a private instructor available at any time for this thesis project. I also would like to thank the late prof. Kimmo Saarinen for taking me into the positron group as an undergraduate student. My thanks also go to professors Pekka Hautojärvi and Martti Puska for sharing their immeasurable knowledge of positron physics with me whenever needed.

I want to thank both the former and the current members of the positron group. You all have been really nice people to work with! Special thanks go to Dr. Klaus Rytsölä, who has been very helpful whenever technical problems have arisen with the measuring equipment or technical knowledge has otherwise been needed.

I also wish to thank my parents and brother for cultivating and supporting my interest in science during all these years. Finally, I wish to thank Elina for understanding why I sometimes had to stay late in the lab and for reminding me what is really important in life.

Espoo, August 19, 2011,

Simo Kilpeläinen

Contents

This thesis consists of an overview and the following publications:

I S. Kilpeläinen, K. Kuitunen, F. Tuomisto, J. Slotte, H. H. Radamson, and A. Yu. Kuznetsov, *Stabilization of Ge-rich defect complexes originated from E centers in $Si_{1-x}Ge_x$:P*, Physical Review B (BR) **81**, 132103, pages 1-4 (2010).

II S. Kilpeläinen, F. Tuomisto, J. Slotte, J. Lundsgaard Hansen, and A. Nylandsted Larsen, *Evolution of E-centers during the annealing of Sb-doped $Si_{0.8}Ge_{0.2}$*, Physical Review B **83**, 094115, pages 1-5 (2011).

III J. Slotte, S. Kilpeläinen, F. Tuomisto, J. Räisänen, and A. Nylandsted Larsen, *Direct observations on the vacancy and its annealing in germanium*, Physical Review B **83**, 235212, pages 1-5 (2011).

IV S. Kilpeläinen, K. Kuitunen, F. Tuomisto, J. Slotte, E. Bruno, S. Mirabella, and F. Priolo, *Vacancy Engineering by He Induced Nanovoids in Crystalline Si*, Semiconductor Science and Technology **24**, 015005, pages 1-4 (2009).

V S. Kilpeläinen, Y.-W. Lu, F. Tuomisto, J. Slotte, and A. Nylandsted Larsen, *Si nanoparticle interfaces in Si/SiO_2 solar cell materials*, arXiv:1106.1753 [cond-mat.mtrl-sci] (2011)

The author, Simo Kilpeläinen, has had an active role in all the phases of the research reported in this thesis. He has been involved in the planning and performing the experiments as well as in the analysis of the experimental data. All positron data has been analyzed by the author. He has also contributed to the interpretation of the results. The author has written publications I, II, IV and V, and performed the experimental part and the data analysis in Publ. III.

1. Introduction

The existence of modern electronics is made possible with the use of semiconducting materials. The striving towards smaller and more powerful components ensures the importance of semiconductor research both in finding new candidate materials for applications and in improving ways in which existing ones are used in the industry. Despite lengthy efforts in finding its successor, silicon is still the most commonly used material in current semiconductor technology. Silicon is a group IV semiconductor and has a forbidden energy gap of 1.1 eV which means that it is an insulator at very low temperatures and a poor conductor at room temperature. Performance-wise silicon is not the best semiconductor but it has other properties which have made it the material of choice in mainstream electronics industry. Firstly, silicon is very easy to grow also in large quantities which makes it cheap and thus gives it by far the best performance-cost ratio among semiconductor materials. In addition to that, silicon also has a stable native oxide, SiO_2, which is very helpful to device industry as it can be used for insulation and passivation layers. [1]

Even though silicon is the mainstream semiconductor in electronics nowadays, the first transistor back in the 1940s was made from another group IV element, germanium [2]. Germanium has a band gap of 0.66 eV so it has better conductivity at room temperature than silicon does. In fact, performance-wise it is a

better semiconductor than silicon. However, silicon's other strengths (cost, native oxide) have allowed it to bypass germanium as the backbone of the electronics industry. After the emergence of silicon, germanium research was all but forgotten for several years, only to surface again in the wake of the new millennium when it became apparent that silicon would soon be reaching its physical limits in the ever-grinding gears of technological development. In the search for silicon's successor germanium has a few trump cards with which it may well beat its competitors. Firstly, carrier mobilities in it are very high thanks to the low effective masses of the carriers. This property makes germanium very potential for high performance applications. In fact, when holes are considered germanium is ahead of all the III-V compound semiconductors in mobility [1]. Secondly, being a group IV element with similar chemical and structural properties to those of silicon makes germanium easy to incorporate into the existing Si-based technology. This can be done with Ge either as a pure material or alloyed with silicon ($Si_{1-x}Ge_x$), the latter bringing more aces on the table in the forms of lattice strain and band gap engineering between the values of pure Si and pure Ge. The strain in $Si_{1-x}Ge_x$ layers is caused by the lattice mismatch between Si and Ge, and it improves the carrier mobilities in the layers. Nowadays, strained $Si_{1-x}Ge_x$ is used to improve the carrier mobilities in high performance transistors [1, 3, 4] but there are plans to utilize pure Ge instead in order to further improve the effect [5].

The electrical (and sometimes also mechanical) properties of a semiconductor are greatly influenced by various kinds of defects present in the material. Point defects such as vacancies (missing atoms) and vacancy-impurity complexes are very common and can be introduced into the material both during growth and device fabrication. It is also possible to purposefully introduce these kinds of defects into a material for example with irradiation. Point defects cause anomalies in the band structure of a semiconductor by adding new energy levels into the forbidden band gap. These levels are able to trap electrons and/or holes and

thus prevent them from filling their desired purpose as charge carriers. Defects can also be useful for example in controlling impurity diffusion. This aspect has become very important due to the need for thinner and thinner highly-doped semiconductor layers in the device industry.

The most common way to remove undesired point defects from a material is to anneal it in high temperatures where the defects become mobile [6]. However, it is not only the defects which become mobile in such a treatment; dopant atoms will also do so. Thus, in applications which need thin doped layers annealing can sometimes be out of the question. In these cases it would be extremely helpful to prevent the formation of defects altogether or at least limit it as much as possible.

In n-type $Si_{1-x}Ge_x$, so-called E centers consisting of a donor atom and a vacancy are very common defects [7, 8]. They are known to act as carrier traps and thus hinder the electrical performance of the material. Increased doping required by present high performance electronics means that the amount of E centers increases as well. Thus, controlling their formation and finding suitable ways to remove them is crucial for the electronics industry utilizing $Si_{1-x}Ge_x$.

The tendency of vacancies to pair with impurity atoms also has a more direct effect; vacancies are very important to impurity diffusion in various semiconductor materials. Depending on the situation, this can be good or bad. In a perfect world impurities would diffuse easily in the thin layer they are intended to be put into and then stop at the interface of the layer and the substrate. In reality, this is hard to achieve without understanding the physics behind the impurity diffusion.

Vacancies may affect impurity diffusion even when the diffusion mechanism does not involve them directly. For example, one of the most commonly used donor dopants in silicon - boron - diffuses in the lattice paired with Si self-interstitials but vacancies still play a large role in its diffusion [9–14]. The self-interstitials are eager to occupy the vacant lattice sites so the presence of vacancies reduces the boron diffusion. Of course, boron itself may also get trapped in the vacancies.

The diffusion-limiting property of vacancies in the case of boron can be very useful when controlling the thickness of a doped layer in silicon.

Vacancy-type defects are a nuisance for people designing novel solar cell materials. In applications where minimizing carrier losses is of utmost importance, getting rid of passivating factors such as vacancies is crucial. In order to improve the light conversion of a solar cell, complex structures such as multijunctions made from several different semiconductor materials, embedded nanowires, or other similar concepts are often used [15–17]. In addition to the increased cost of the device, the drawback of this is that a complex material provides interfaces near which vacancies like to accumulate.

In this thesis, vacancy-type defects in three group IV semiconductors - Si, Ge, and $Si_{1-x}Ge_x$ - are studied using positron annihilation spectroscopy (PAS). This technique is based on detecting the radiation created by annihilating positron-electron pairs. Positrons are able to get trapped into neutral or negative vacancy-type defects and thanks to that PAS is a very sensitive tool for detecting and analyzing such defects. Positrons can reveal information about the size, concentration, charge state and even the chemical surroundings of vacancies [18].

The first two publications deal with vacancy-donor complexes in $Si_{1-x}Ge_x$. In Publ. I, the evolution of E centers during isothermal annealing of P-doped $Si_{1-x}Ge_x$with three different Ge contents ranging from 10 to 30% is studied. An Arrhenius-like model is used to determine activation energies for the process and values around 1 eV are obtained. Publ. II is an investigation of the effects of isochronal and isothermal annealing of E centers in Sb-doped $Si_{1-x}Ge_x$. In this case, the Ge content is kept constant at 20% and the dopant concentration is varied. The average amount of Ge atoms around the E centers is shown to increase during the annealing and Ge clustering is detected in the lattice after the anneal is over.

Even though Ge was the material used in the first ever transistor, it has been

studied considerably less than silicon. In Publ. III, Ge is irradiated with protons at a low temperature and then studied with an *in situ* annealing experiment utilizing positron lifetime spectroscopy. Two different annealing stages are observed at 100 K and at 200 K. The first one is attributed to the Frenkel pair and the second to the monovacancy. Divacancies are found to be stable at room temperature as their presence is confirmed in measurements performed after storing the irradiated sample at room temperature in atmospheric pressure.

The other two publications in this thesis concentrate on silicon but from completely different viewpoints. In Publ. IV, the use of He implantation as a means to control and limit B diffusion in Si is studied. Nanovoids generated by the He implantation process are observed and interstitials created during a subsequent B implantation are found to get trapped in these defects. Publ. V deals with a novel solar cell material consisting of Si nanocrystals embedded within an SiO_2 matrix. The nanocrystals are formed by annealing Si/SiO_2 multilayers at 1100°C in N_2. Interfaces between the nanocrystals and the SiO_2 matrix are studied with positrons and photoluminescence. Nanocrystal formation is found to be optimized in samples with 2 nm thick Si layers.

2. Semiconductor and defect physics

Despite their name, semiconductors are actually closer to insulators than metals when their electronic properties are considered. Their energy band structure is very complex but it is usually simplified into a model with two energy bands – the valence and the conduction band – which are separated by a band gap typically ranging from tenths of eVs up to a few eVs. At 0 K, the valence band is completely filled and the conduction band empty, and thus the material is insulating. However, at elevated temperatures some of the electrons are thermally excited from the valence band into the conduction band where they can act as charge carriers. The holes left in the valence band in place of these excited electrons are also able to carry electric current.

Intrinsic semiconductors are typically not very useful in electronics industry due to the fact that most of them are weakly conducting at room temperature. The conductance, however, can be drastically improved by doping i.e. introducing impurity atoms into the semiconductor. These impurities can either donate electrons to the conduction band or accept them from the valence band. In n-type doping, the amount of charge-carrying electrons is increased by adding impurities with an extra electron into the material. p-type doping, respectively, involves adding impurities with one less electron. When it comes to group IV semiconductors, n-type doping is typically achieved with group V elements such as P, As

or Sb whereas B is the most common element for p-type doping.

Point defects such as vacancies or interstitials are crucial to the electronic properties of a semiconductor since they can act as compensating donors or acceptors, and by doing so reduce the carrier concentration. This happens since these defects are able to form new energy levels, which act as traps for either electrons or holes, in the forbidden band gap.

In this Chapter, some basic principles of semiconductor defect physics, especially from the point of view of group IV semiconductors, are discussed. More details can be found in Refs. [6, 19–22].

2.1 Silicon and germanium

Silicon and germanium are the two elemental semiconductors belonging to group IV in the periodic table of elements. Both of these materials have a cubic diamond crystal structure where each atom is covalently bonded to its four neighbors.

Silicon has already been for decades and still is the most important semiconductor material in electronics industry. It has been able to maintain the position thanks to a few key properties such as a stable native oxide, a large band gap and last but not the least, easy and cheap manufacturability [23, 24]. Diligent efforts in Si research have paid off in tremendous computing speed increases as manufacturing smaller and smaller chips has become possible.

Germanium was the material chosen for the first ever transistor but after silicon's emergence it has only had a small niche in semiconductor industry. During the last decade or so germanium research has received more interest, though, since we are starting to approach the physical limits of silicon in the never ending race for more powerful microprocessors. Effective masses for both electrons and holes

are lower in germanium than in silicon, leading to higher carrier mobilities. This in turn means that it is possible to build more powerful devices by utilizing Ge instead of Si. The drawbacks of Ge - high cost, poor processability and lack of stable native oxide - are preventing its use in mainstream electronics but it is utilized for example in radiation detectors as well as solar cells used in space applications [25]. Building a modern field effect transistor (FET) entirely out of Ge is a distinct goal for many research groups [5] but there are still obstacles to be overcome in the post-growth stages of the device manufacturing process.

A compromise between germanium's performance and silicon's availability and easiness of use is to utilize both as an alloy, silicon germanium ($Si_{1-x}Ge_x$). By using $Si_{1-x}Ge_x$, it is possible to improve the performance of existing Si-based electronics without having to resort to large-scale re-design [1]. Via adjustment of the Si/Ge ratio of the material, it is possible to tune the band gap freely between the values of pure Si and pure Ge. The band structure itself, however, remains Si-like for Ge contents up to 85 % and helps with the integration into Si-based systems. Even though the lattice constants of Si and Ge are quite close to each other, the difference is enough to introduce strain in $Si_{1-x}Ge_x$ lattices. This strain changes the energy band structure by splitting the six conduction band valleys of Si in energy and doing similarly for the top of the valence band by separating the bands for heavy and light holes. These energy band changes further improve carrier mobilities by decreasing scattering [26, 27]. Strained $Si_{1-x}Ge_x$ layers are used to improve carrier mobilities in high performance transistors [1, 3, 4]. Also, the realization of the 32 nm scaling node [28] was made possible by strain and heterojunction engineering provided by $Si_{1-x}Ge_x$ [29]. It is also possible to grow relaxed $Si_{1-x}Ge_x$ *e.g.* by utilizing buffer layers with increasing Ge content. While relaxed $Si_{1-x}Ge_x$ does not have the strain-induced carrier mobility improvement, it still has its uses. It can for example be used for creating strained Si on relaxed $Si_{1-x}Ge_x$ -heterostructures and for achieving relaxed $Si_{1-x}Ge_x$-on-insulator substrates [30].

2.1.1 Novel solar cells based on Si nanocrystals

Silicon has been the mainstream material for solar cell industry since the discovery of the Si-based photocell [31]. The Si solar cells have several advantageous properties; they are easy to produce in masses, relatively cheap, can be used in various applications, and Si is a non-toxic material. However, the energy conversion efficiency is just approaching 25% for the very best commercial Si solar cells, and the typical mainstream cells have efficiencies of around 15% [32]. The classical theoretical limit for single Si solar cells, based on the energy spectrum of the Sun and the band gap of Si, is not that great either: 31% [33]. Thus, the most common procedure for producing very efficient solar cells is to use composite structures consisting of layers made from different materials sensitive to different wavelengths of sunlight [15, 16]. These multilayered solar cell structures are, however, very complex to produce and thus expensive which makes them unsuitable for mainstream use. Since traditional energy sources such as coal and oil are gradually running out and on top of that pollute the Earth's atmosphere, researchers are very eager to find ways to better harness the energy of the Sun. A promising concept was discovered a couple of years ago when Klimov and his colleagues discovered that silicon nanocrystals could convert a single photon into more than one excitons [34]. A solar cell utilizing this property could be a workaround for getting beyond silicon's theoretical energy conversion efficiency without having to resort to expensive materials. Promising candidates for such solar cells could be SiO_2 layers embedded with Si nanocrystals. Such layers have been prepared and studied with several techniques [35–41]. The results have been promising so far but there is still much work to be done before these solar cells can become commercially available. The biggest problem is that the interface between the nanocrystals and SiO_2 tends to have carrier traps in it, thus decreasing the light conversion efficiency.

2.2 Point defects in elemental semiconductors

As the name suggests, point defects consist of various "zero-dimensional" i.e. non-extended defects present in the lattice. They can be categorized into three different subgroups:

a) Vacancies e.g. atoms missing from regular lattice sites.

b) Interstitial defects in which an additional atom is located between regular lattice sites. The atom can either be one of the host lattice species or an impurity.

c) Substitutional defects in which an impurity occupies the lattice site of one of the regular lattice atoms.

In addition to the simple forms described above, point-like defects can also be found as larger complexes and clusters such as divacancies, vacancy-impurity pairs and vacancy clusters.

Point defects can interact with others in various ways and these interactions can be described with the following list of reactions [22]:

$$I + \mathrm{S} \leftrightharpoons (\mathrm{S}{-}I) \text{ or } I + \mathrm{S} \leftrightharpoons \mathrm{S}_i, \tag{2.1}$$

$$V + \mathrm{S} \leftrightharpoons (\mathrm{S}{-}V), \tag{2.2}$$

$$I + (\mathrm{S}{-}V) \leftrightharpoons \mathrm{S}, \tag{2.3}$$

$$V + (\mathrm{S}{-}I) \leftrightharpoons \mathrm{S} \text{ or } V + \mathrm{S}_i \leftrightharpoons \mathrm{S}, \tag{2.4}$$

$$I + V \leftrightharpoons 0. \tag{2.5}$$

Here S refers to an impurity atom, V to a vacancy, I to an interstitial atom and S_i an impurity atom at an interstitial site. S–D refers to a complex consisting of an impurity atom and a defect D ($D = V$ or I).

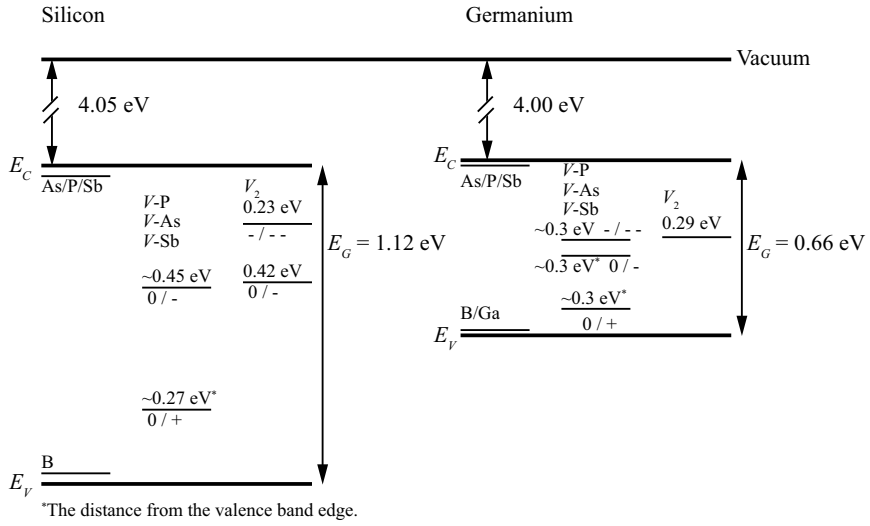

Figure 2.1. *Ionization level positions of some common defects in the Si and Ge band gaps. The values refer to the distance from the conduction band edge E_C, except when a value is marked with an asterisk in which case it refers to the distance from the valence band edge E_V. The exact positions of the vacancy-donor defects depend on the donor atom type. The data is from Refs. [42–45].*

Point defects are typically harmful in semiconductors since they are able to introduce new energy levels into the forbidden band gap. These levels then act as traps for carriers, thus reducing the active carrier density. Levels which trap electrons from the conduction band are called acceptor levels and ones that trap holes from the valence band donor levels. The defect levels are usually referred to by the charge transition associated with them. For example, the single acceptor level is referred to as (0/-) and the single donor level as (0/+). The charge states of defects are determined by the position of the Fermi level E_F. If E_F moves up (towards the conduction band), the defects become more negative and vice versa. An energy level diagram of some of the most common defects in Si and Ge can be found in Fig. 2.1.

2.2.1 E centers

One of the most important point defects in group IV semiconductors is the E center which is a complex consisting of a vacancy and a group V donor atom (P, As or Sb). In addition to affecting the electrical properties of the material, E centers have also been shown to influence impurity migration in Si [46, 47]. The electronic levels of E centers are shown in Fig. 2.1. In pure Si, two E center -related energy levels have been found: an acceptor level at E_C-0.45 eV [48–50] and a donor level at E_V+0.27 eV [42], where E_C and E_V are the conduction and valence bands of the material, respectively. In Ge, the E center has two acceptor levels and one donor level [51–53].

The recent interest in $Si_{1-x}Ge_x$ as a material in semiconductor technology combined with the importance of the E center has led to numerous studies focusing on E centers in $Si_{1-x}Ge_x$ [7, 54–58]. While these studies have contributed significantly to the understanding of E centers in $Si_{1-x}Ge_x$ the fundamental picture of the defects is still lacking. Especially experimental documentation is insufficient and the existing works are largely based on high temperature dopant redistribution measurements which always involve the inevitable risks of modifying the delicate $Si_{1-x}Ge_x$ matrix itself.

The deep level transient spectroscopy studies of Monakhov *et al.* report on defect characteristic electronic levels in n-type strained proton irradiated $Si_{1-x}Ge_x$ samples [7, 54]. Kringhøj *et al.* have contributed to the cause by showing the distance of the E center acceptor level to the conduction band edge to be the same regardless of the Ge content in relaxed $Si_{1-x}Ge_x$ [55]. In an earlier positron annihilation study, the E center in $Si_{1-x}Ge_x$ has been shown not to prefer Si or Ge atoms as nearest neighbors after proton irradiation treatment [56]. However, another positron annihilation study showed that annealing strained $Si_{1-x}Ge_x$ layers increases the average number of Ge atoms around the E centers and the subse-

quently formed V-P-Ge complexes are by 0.1–0.2 eV more stable than the simple V-P pairs [58]. In this thesis, the effect of annealing on E centers and their Ge decoration is studied in P-doped (Publ.I) and Sb-doped (Publ. II) $Si_{1-x}Ge_x$.

2.3 Diffusion

In addition to directly influencing the electrical properties of semiconductors, point defects often also have an indirect effect in the form of controlling impurity (dopant) diffusion. While it is possible for an impurity to diffuse by simply exchanging places with a lattice atom (direct-exchange), the process is considerably slower than indirect diffusion mediated by vacancies or interstitials. In vacancy-mediated diffusion the impurity atom hops into a neighboring vacant lattice site. If the vacancy and the impurity are attracted to each other, it is possible for them to diffuse through the lattice as a pair. In interstitial-mediated diffusion, the interstitial atom kicks an impurity atom from a lattice site into an interstitial position. The kicked-out impurity can then proceed to diffuse as an interstitial until it finally settles to a new lattice site by kicking another atom out of it into an interstitial position [22, 59]. Like in vacancy-mediated diffusion, the impurity can also diffuse through the lattice as a pair with the interstitial [60–62].

Diffusion of impurities depends largely on three quantities: temperature, impurity concentration and the type of impurity atoms. Increasing the temperature typically strengthens diffusion. Large impurity concentrations also improve diffusion as the concentration gradient becomes larger. The type, or rather the size of the impurity often dictates the diffusion mechanism. Small impurities may move rather freely between the lattice atoms and thus prefer the interstitial mechanism. Larger atoms on the other hand need more empty space to maneuver and thus favor the vacancy mechanism. This is well displayed with the group V donors in Si: P diffuses almost entirely via interstitials, As uses a mixture of vacancy- and

interstitial-mediated diffusion and Sb diffuses via the vacancy mechanism [63, 64].

Dopant diffusion is not always a good thing for device industry. Uniform distribution of dopants in a layer would be very hard to achieve without diffusion but on the other hand preventing the dopants from escaping the target layer would be far easier. A good example of the latter is p-type doping of Si layers with B. During B implantation, Si interstitials are also formed. Since B diffusion is mediated by interstitials in Si, these new interstitials enhance it and thus make controlling the thickness of the doped layers very challenging. This enhanced diffusion is called transient enhanced diffusion [60].

2.4 Defects introduced by processing of semiconductors

Point defects are always present in crystalline materials. However, in the case of group IV semiconductors most of them are introduced during post-growth processing stages such as doping. Because of this, making a semiconductor device is balancing between improving the material properties with doping and degrading them with the introduction of defects. For example, common processes such as ion implantation and oxidization are known to generate vacancies and interstitials. These defects are especially problematic in thin films required by modern electronics since the best way to remove them – annealing at a high temperature – also enhances impurity diffusion and thus broadens the impurity profile.

The very same ways of unwillingly introducing defects into semiconductor materials can also be used to produce well-defined defects for research purposes. In Publ. III, Ge has been proton-irradiated at low temperatures in order to study the generation and annealing of simple vacancy-type defects. Vacancies have a low formation energy in Ge and may thus play a large role in both self- and impurity diffusion [65]. They may also passivate dopants by forming E centers. Even

though vacancies are very important for the electronic properties of Ge, especially experimental studies on vacancies are very scarce, largely due to Ge being in silicon's shadow for decades. Even such a trivial-sounding concept as the stability of a divacancy in room temperature has been a topic of controversy. Theoretical calculations have suggested it to be stable [66] and it has been suggested to have electronic levels in the upper half of the band gap at $E_c - 0.29$ eV [51, 67, 68]. However, experimental evidence has been lacking until now. Divacancies were observed at room temperature in a recent positron annihilation study [69] and again in Publ. III of this thesis.

Boron implantation is currently the most common way to produce shallow, heavily p-type regions in Si. The demand for thinner and more heavily doped layers has awakened new concerns in device manufacturers as the carrier concentration is limited both by electrical deactivation of the dopants and their diffusion out from the target layer. During B implantation, a high number of Si self-interstitials and vacancies are formed. The Si interstitials are doubly harmful as B undergoes transient enhanced diffusion via them [60, 70] and also forms boron-interstitial clusters (BICs) with them [9, 10, 70, 71]. So far, there is no commercially suitable technique to control these phenomena.

One promising technique to control B diffusion in crystalline Si – He implantation – is studied in Publ. IV. Interstitials have been found to be suppressed by this technique both in crystalline and in pre-amorphized Si [72–75]. The He implantation causes a large amount of vacancies to form at the projected range R_p of the He ions. By subsequently annealing the material, it is possible to turn these vacancies into empty voids [76, 77] which act as sinks for the self-interstitials [78]. Unfortunately, in addition to this the voids can introduce deep levels into the band gap which then act as recombination centers for carriers and lower the carrier concentrations [79]. Recently, another layer of smaller "nanovoids" has been discovered at approximately $R_p/2$, rekindling the interest in the He implantation technique. These nanovoids have been suggested to cause significant reduction

in B diffusion in the He implanted samples [73]. With the nanovoids, the detrimental effect of the deep void layer at R_p can be avoided since B never reaches it. Positron annihilation studies of both self- and He-implanted Si have also confirmed the existence of vacancy clusters in the $R_p/2$ region but systematic studies on the formation kinetics and the size of these nanovoids are yet to be carried out.

2.5 Semiconductor defect characterization methods

There are various methods for detecting and characterizing defects in semiconductors. In this work, positron annihilation spectroscopy (PAS) is used for this purpose. The strength of the method lies in the ability to selectively detect and identify defects at various depths (depending on equipment) without destroying the sample structure in the process. The detectable defect concentrations (from 10^{15} cm^{-3} to 10^{19} cm^{-3}) fall nicely within the range of usual dopant concentrations in semiconductors. Temperature- and illumination-dependent measurements are also possible. There are no specific requirements for samples other than size for practicality purposes so insulating materials and even liquids can be measured. The biggest drawback of PAS is that it requires elaborate equipment and involves dealing with radioactive substances. Furthermore, it is only sensitive to negatively charged or neutral defects involving open volume which limits its use in some cases. The measurement times are also rather long unless very strong positron sources are used so *in situ* process monitoring with positrons is impossible or at least very hard to do. More details on PAS can be found in Chapter 3.

When it comes to detecting defect-related deep levels in the band gap, the most commonly used technique is deep level transient spectroscopy (DLTS) [80, 81].

The method can only be used on p-n junctions or Schottky barrier diodes but fortunately the latter is easy to form by simply depositing a thin metal film at room temperature over the studied semiconductor [81]. It is also possible to measure real device structures with DLTS provided they meet the requirements [82]. The technique is based on measuring the depletion capacitance of the space-charge region in a p-n junction or a Schottky barrier diode. The depletion capacitance changes in the presence of deep levels caused by various defects such as vacancies, interstitials or defect complexes. In conventional DLTS, the capacitance is measured while the temperature of the sample is varied slightly. Isothermal measurements are possible with Laplace DLTS which is a high-resolution variant of the technique [83]. With DLTS, it is possible to determine the position of the defect level in the band gap, defect concentration and thermal emission properties of the defect. From the measurements it is also possible to obtain the activation energy, concentration profile and carrier capture cross sections of the defect(s) [81]. DLTS is sensitive to deep level concentrations about two orders of magnitude less than the carrier concentration in the sample [84]. However, the sensitivity of DLTS also involves a problem; the technique will not work if the carrier concentration is too high and the sample is very conducting. Typically samples with dopant concentrations higher than 10^{18} cm^{-3} are problematic from this standpoint. Another drawback of DLTS is that it only provides information on the position of the defect level relative to the band gap and thus direct identification of the defect is often impossible [80]. A workaround to this is to use DLTS in conjunction with another characterization technique such as PAS or electron paramagnetic resonance (EPR).

EPR is another widely used technique for semiconductor defect studies [85]. It has, for example, been successfully used in studying intrinsic defects in Si by Watkins [6, 86]. In EPR measurements, an alternating magnetic field perpendicular to the steady field is applied on the sample and microwave photons are emitted into the sample at a constant frequency. The varying magnetic field

causes magnetic dipole transitions between the Zeeman-split energy levels of the studied object which can be a point defect, an ion, a molecule or some other chemical species. When the incident photon energy corresponds to the energy separation between the Zeeman-split levels, resonant absorption of the photons is observed [20]. EPR is – like the name suggests – only sensitive to paramagnetic objects and thus cannot usually be applied to defects with an even number of electrons. Electrically active defects, however, often have at least one charge state at deep levels in the band gap in which an odd number of localized electrons with a net spin moment causes paramagnetism [87]. It is also possible to create paramagnetic states by illumination [88]. Elements with many stable isotopes – such as Ge – are problematic for EPR as paramagnetism is different for each isotope. This leads to very complex spectra from which it is difficult (or often impossible) to distinguish the defect signals. In the cases EPR can be applied, it is very sensitive and can detect paramagnetic centers at concentrations as low as 10^8 cm^{-3}.

Photoluminescence (PL) differs from DLTS and EPR considerably since it is an optical technique. Like PAS and EPR, it is a nondestructive method and is thus well-suited for device industry [84]. PL is based on the luminescence generated by the radiative recombination of excess carriers in a semiconductor. These excess carriers are usually produced by illuminating the sample with a laser beam. The carriers can also be produced by a high-energy electron beam from *e.g.* a scanning electron microscope. If electrons are used instead of light, the technique is called cathodoluminescence (CL). The energies of the observed luminescence bands give information about the defect energy levels and the intensities are related to defect concentrations, albeit in a rather indirect way [84]. Both PL and CL are usually performed at low temperatures due to the fact that at elevated temperatures excess carriers tend to diffuse onto the surface and recombine there without light emission. The luminescence techniques are both extremely sensitive and can in optimal conditions detect even a single luminescent center in the sample [89].

X-ray diffraction (XRD) techniques are also commonly used for detecting defects in semiconductors. They are nondestructive and require no sample preparation. Furthermore, it is possible to probe the whole structure of a sample with an XRD scan. These properties make X-ray -based techniques very attractive to device industry. XRD techniques are limited by their low resolution (typically tens of nm even for high-resolution variants) and thus are only applicable to materials with low defect densities [90]. They are, however, very good for detecting extended defects such as dislocation lines in manufactured devices. The main drawback for all XRD techniques is that they require highly ordered crystalline samples and measurement times are often very long (from hours up to days). Also, data from reference samples are always needed for the interpretation of XRD results.

In addition to methods that are directly used to detect and identify defects, there are some techniques that can be used as complementary tools for defect characterization in semiconductors. Hall effect measurement is a simple way for obtaining the carrier concentration, resistivity, carrier mobility and carrier type. The presence of deep scattering centers can be revealed by reduced carrier mobility in Hall measurement results. Spreading resistance profiling (SRP) can be used to measure the resistance as a function of depth at the cost of very complex sample preparation [80, 91]. Secondary ion mass spectroscopy (SIMS) is a destructive method for quantitatively analyzing the dopant and impurity profiles in a sample and is sensitive to dopant densities down to 10^{15} cm^{-3} [80, 91–93]. In SIMS measurements sample material is removed by sputtering and then analyzed with a mass analyzer. Naturally it cannot detect vacancies which have no mass but it can provide information about them indirectly for example via diffusion profiles and dopant accumulation.

3. Positron annihilation spectroscopy

Positron annihilation spectroscopy (PAS) is a powerful tool for studying vacancy-type defects in different materials [18, 94, 95]. The method is based on positrons annihilating with electrons in the sample material and subsequent 511 keV annihilation gamma photons being detected. A positron is able to probe the sample very effectively for open volume defects such as vacancies with neutral or negative net charge and gets trapped in such defects. PAS not only detects vacancy-type defects but also gives information about their size, concentration, charge-state and even chemical surroundings. Fast positrons obtained directly from a positron source can be used for bulk studies whereas slow positron beams are needed in order to investigate thin structures such as semiconductor films. The positron annihilation technique is commonly used for defect studies in two different modes. Positron annihilation lifetime spectroscopy (PALS) is based on measuring time differences between the emission of a positron from the source and its annihilation within the sample. A positron trapped into a vacancy typically lives longer than a free one, leading to an increase in positron lifetime. Positron Doppler broadening spectroscopy on the other hand focuses on measuring the energies of the annihilation photons and is very sensitive to the chemical surroundings of the positron traps.

3.1 Positrons in solids

Positrons can be easily obtained either as a product of radioactive β^+ processes or via pair production methods. The most commonly used positron source is ^{22}Na which decays into ^{22}Ne via the β^+ process and has a half-life of 2.6 years [18]. Simultaneously with the positron emission ^{22}Na produces a characteristic gamma photon of 1.274 MeV which can be used as a signal for the positron emission in PALS.

When a positron enters a solid, it loses its momentum very rapidly and thermalizes within a few picoseconds [94–96]. After thermalization it diffuses for a few hundreds of picoseconds before finding an electron and annihilating. If the positron finds neutral or negatively-charged open volume during this diffusion, it may get trapped. Since the local electron density is lower in open-volume defects, the probability for the positron to annihilate at a given moment of time decreases and thus its lifetime becomes longer than the bulk lifetime (the lifetime of a positron in a defect-free lattice). The positron lifetime can be determined e.g. by measuring the time difference between the detections of the characteristic emission gamma photons from the positron source and one of the 511 keV annihilation photons.

The annihilating positron-electron pair follows the law of momentum conservation. In practice this means that whatever momentum the pair (practically only the electron since the positron is thermal) had during the moment of annihilation is transferred to the two annihilation photons. The momentum is then seen as a Doppler shift in the energy spectrum of the 511 keV annihilation line and also as a small angular deviation between the emission directions of the two annihilation photons. Since valence electrons typically have considerably lower momenta than core electrons, the Doppler broadening spectrum gives information about the type of the annihilating electrons. Core electrons are lacking and valence annihilation

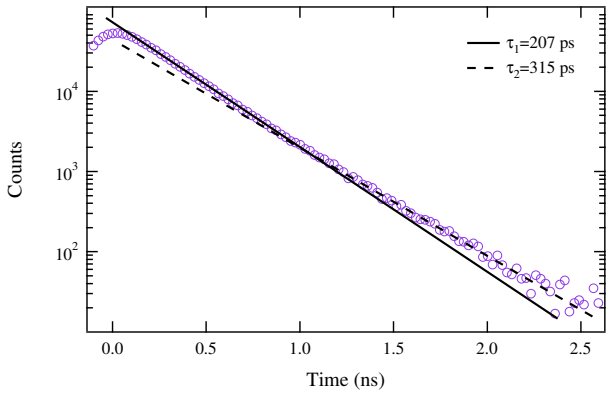

Figure 3.1. *Positron lifetime spectrum of proton irradiated Ge measured at RT. The lines are fits of the two positron lifetime components found in the experimental data.*

dominates in vacancies, leading into a narrower annihilation line compared to that of defect-free material. The high-momentum part of the spectrum comes almost entirely from the core electrons of atoms near the vacancy and thus gives information about the chemical surroundings of the defect.

Thorough reviews on the measurement techniques and the theory of positrons in solids are available in Refs. [18, 94–96].

3.2 Positron lifetime spectroscopy

In positron lifetime measurements, the time differences of the positron emission signal (typically a gamma photon emitted by the positron source simultaneously with the positron; in the case of ^{22}Na a 1.27 MeV photon) and one of the 511 keV annihilation photons are measured. These differences are then collected into a histogram also known as the positron lifetime spectrum. An example of a

typical lifetime spectrum is presented in Fig. 3.1. The raw spectrum is of the form $n(t) = \sum_i I_i \exp(-t/\tau_i)$ and is usually analyzed as a sum of exponentially decaying components convoluted with the (typically) Gaussian resolution function of the spectrometer. The indices i correspond to the different lifetime components with lifetimes τ_i and intensities I_i.

Sometimes the decomposition of a spectrum into lifetime components fails due to, for example, poor resolution of the spectrometer or two components being too close to each other to be separated. Even in these cases, the data can be evaluated with the help of the average positron lifetime which is of the form

$$\tau_{ave} = \sum_{i=1}^{N} I_i \tau_i, \tag{3.1}$$

when N separate lifetime components are present. The average lifetime coincides with the center of mass of the lifetime spectrum and is thus independent of the spectral decomposition. An average positron lifetime higher than that of defect-free bulk (τ_B *e.g.* 218 ps for Si) is an indication of vacancy-type defects in the material [94]. Due to the nature of τ_{ave}, it is possible to reliably measure changes as small as 1 ps. The average lifetime can also be used to determine the vacancy concentration in the sample according to the conventional positron trapping model [95], provided that the decomposition of the spectrum can be performed. The vacancy concentration c_D relates to the trapping rate κ obtained from the trapping model according to

$$\kappa = \mu_D c_D, \tag{3.2}$$

where μ_D is the trapping coefficient, roughly 1–2$\times 10^{15}$ s^{-1} [18].

Positron states in the sample j can be described with a characteristic lifetimes $\tau_j = 1/\lambda_j$, where λ_j are the corresponding positron annihilation rates. If there is only a single defect type with a specific lifetime τ_D present in the sample and the trapping of positrons into these defects is not saturated, the decomposition of the positron lifetime spectrum yields two components. As long as no trapped

positrons escape the defects before annihilating, the longer measured positron lifetime component $\tau_2 = \tau_D$ directly gives the positron lifetime in the defect whereas the shorter component is the modified bulk lifetime $\tau_1 = (\tau_B^{-1} + \kappa)^{-1}$. The trapping rate κ derived from the kinetic trapping model is [95]

$$\kappa = \frac{\tau_{ave} - \tau_B}{\tau_D - \tau_{ave}} \lambda_B. \tag{3.3}$$

In this thesis, all positron traps measured with lifetime spectroscopy are deep enough for no detrapping to occur but in the case of shallow traps a different trapping model must be used. More information on the trapping models can be found in the appendix of Ref. [95].

3.3 Doppler broadening spectroscopy

In positron Doppler broadening measurements, the interest lies in the annihilation photons and namely their energies. Thanks to the momentum distribution of annihilating electrons, the nominal annihilation line at 511 keV is Doppler broadened as shown in Fig. 3.2. Since the energy resolution of typical high purity Ge detectors used in positron Doppler broadening measurements is of the same order of magnitude (1.3 keV at 511 keV) as the Doppler broadening of the spectrum, using the exact energies of the annihilation photons makes no sense. Thus, so-called annihilation lineshape parameters (S and W) are used instead. These parameters are defined as ratios of a certain area of the annihilation peak to the total area of the peak. The S parameter describes the fraction of positrons annihilating with low momentum electrons (near the center of the peak), with approximately $|p_L| < 0.4$ a.u. ($|E_\gamma - 511 \text{ keV}| < 0.75$ keV), while W is the fraction annihilating with electrons corresponding to the high momentum "wings" of the 511 keV peak, with approximately 1.6 a.u. $< |p_L| <$ 2.4 a.u. (2.9 keV $< |E_\gamma - 511 \text{ keV}| <$ 4.4 keV).

In a vacancy, the amount of core electrons is reduced so generally an elevated (lowered) S (W) is a hint of vacancy-type defects in the sample. However, this is not always the case as positron Doppler broadening spectroscopy is also sensitive to the chemical surroundings of the annihilation site, which obviously makes things more complicated. In most cases, though, the neighboring atoms mainly influence the W parameter and S is left virtually unchanged.

Similarly to positron lifetime spectroscopy, the trapping rate is proportional to the measured annihilation parameters:

$$\kappa = \frac{S - S_B}{S_D - S}\lambda_B = \frac{W - W_B}{W_D - W}\lambda_B, \tag{3.4}$$

where the indices D and B correspond to the annihilation parameter values at the defect and in defect-free bulk, respectively.

When one wants to focus on the chemical surroundings of vacancies or other positron traps, it is possible to perform the Doppler broadening measurements with two detectors in coincidence mode. With this technique, the peak-to-background ratio of the spectrum can be drastically improved – up to $\sim 10^6$ (see Fig. 3.2). This enables a more accurate measurement of high-momentum (core) electrons which are characteristic for different elements [97]. In a coincidence Doppler broadening measurement, the results are collected in a two-dimensional matrix. The conservation of energy gives $E_1 + E_2 = 2m_0c^2 - E_b$, where E_b is the binding energy of the electron and positron in a solid, so the annihilation events are found on the diagonal of the matrix. Due to the finite resolution of the system, only counts where the sum of the photon energies is within 2 keV to $2m_0c^2$ are accepted to the final 1D spectrum. By doing this, the resolution of the measurement system is improved by a factor of $\sim\sqrt{2}$. A resolution function for the measurement system can easily be obtained from the other diagonal $E_1 - E_2 = constant$, making direct comparisons of experimental data and theoretical calculations possible [98].

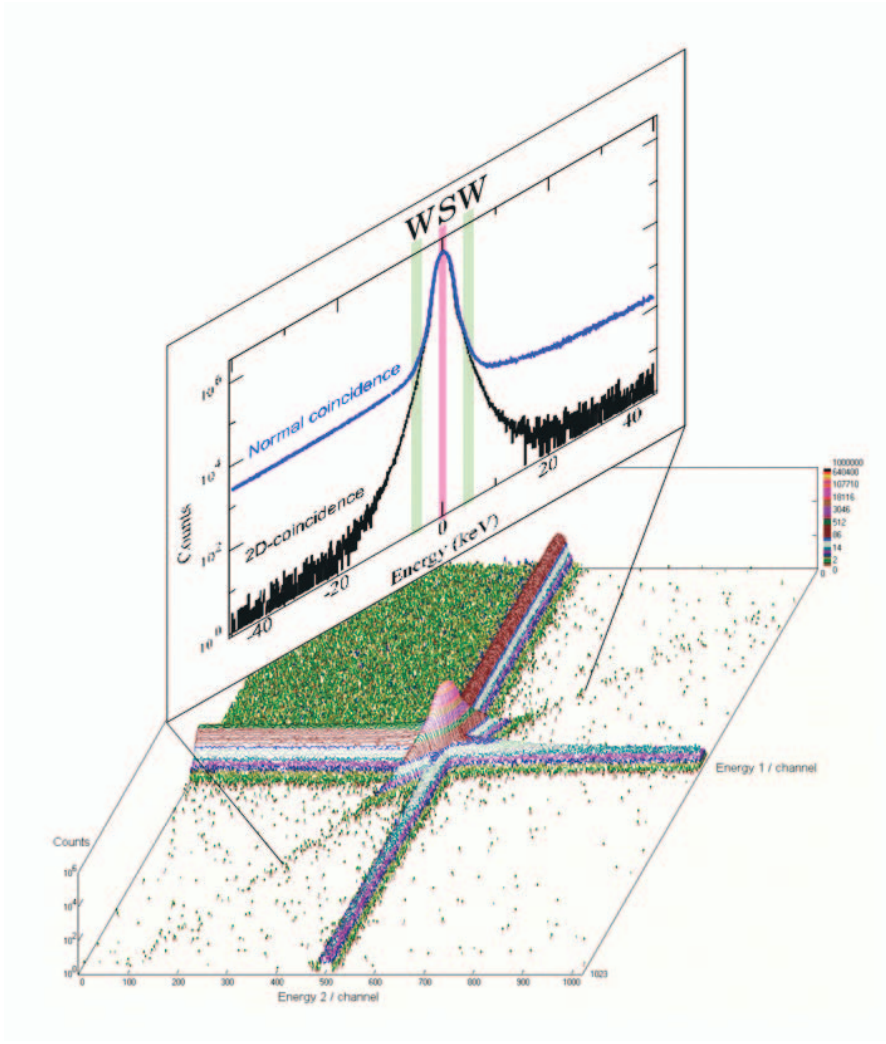

Figure 3.2. *A two-dimensional Doppler spectrum obtained from a coincidence measurement, and the conventional one-dimensional spectrum obtained from it. Typical S and W parameter windows are also presented in the 1-D spectrum.*

3.4 Measurement setups

Positrons used in measurements are divided into two categories: fast and slow [18, 94, 95]. Fast positrons are those directly obtained from a positron source *e.g.* ^{22}Na and are thus easily available for measurements. However, they are only suitable for measuring bulk samples as they would pass through a thin sample. When measuring layers of a few microns or thinner, slow positrons moderated into a monoenergetic beam are needed.

3.4.1 Fast positron measurements

The typical sample configuration for fast positron measurements consists of a positron source sandwiched between two identical sample pieces [18]. This configuration ensures that all positrons aside from those annihilating in the source material end up in the sample. The stopping profile of fast positrons from β^+-active sources is exponential and depends on the source as well as the sample. For the most commonly used positron source, ^{22}Na, the maximum energy of the positrons is $E_{max} = 0.54$ MeV [94]. This typically corresponds to a positron mean stopping depth of 100 μm. For example, in Si the mean stopping depth for positrons from a ^{22}Na source is 110 μm [94]. Thus, fast positrons are best suited for probing homogenous bulk samples with thicknesses of several hundreds of micrometers and up.

With fast positrons, the usual measured quantity is positron lifetime since it gives more information about the defects (size, concentration) than Doppler broadening. A typical positron lifetime spectrometer has two detectors consisting of a fast scintillator and a photomultiplier tube. In a conventional analog setup, the output pulses of the detectors are amplified and fed to constant fraction discriminators which turn them into timing pulses. The timing pulses are then used by a time-amplitude converter to produce pulses whose amplitudes are proportional

to the single positron lifetimes. These lifetime pulses are collected by a multichannel analyzer and stored into a positron lifetime spectrum. Nowadays, the improved performance of analog-to-digital converters (ADCs) has made digital positron lifetime measurements possible. In a digital setup, the only analog electronics remaining are the detectors whose signals are fed directly into a digitizer card plugged into a computer. The detector output pulses are then digitized and pulse shaping as well as timing are done by software. In this work, all the lifetime measurements were performed with a digital setup.

A typical positron lifetime spectrum has 1–2 million counts. Prior to doing the decomposition into lifetime components, contributions to the spectrum by annihilations in the source material, the Al- or Ni-foil covering the source and as positronium are subtracted from the spectrum. The source corrections are determined from a reference sample for which the exact positron lifetime is well-known.

One of the lifetime spectrometers used in this thesis was installed on the beamline of a tandem Van de Graaff accelerator [99]. This, along with the He cryocooling of the sample holder, made it possible to perform the *in situ* proton irradiation experiments introduced in Publ. IV. Typically, positron lifetime spectrometers are fitted with a sample holder with resistive heating and liquid He or N cooling for controlling the sample temperature. Also, sometimes a high-resolution Ge detector is used to perform a Doppler broadening measurement at the same time a lifetime spectrum is collected.

3.4.2 Slow positron beams

When measuring samples or structures considerably thinner than the 100 μm required by fast positrons, measurements need to be done with a slow positron beam. In a slow positron beam, fast positrons are first moderated by a material with a negative work function for positrons (often tungsten) [18]. The negative work function means that positrons which thermalize within the moderator foil

are spontaneously emitted from it. Unmoderated positrons are discarded and the moderated ones are then accelerated in an electric field, resulting in a tunable-energy beam of slow positrons. Typically, the acceleration voltages vary from 0.5 up to a few tens of kilovolts. In this thesis, beams with maximum positron implantation energies of 35 keV and 25 keV were used.

Since the time taken by the moderation process is random for each positron, it is no longer possible to use the characteristic emission gamma photons of the positron source for obtaining positron lifetime information. Thus, only Doppler broadening measurements are possible on a conventional slow positron beam. For this purpose, one of the beams used in this thesis was fitted with two high-purity Ge detectors and the other one with a single detector. In some measurements on the dual-detector beam, the detectors were used in coincidence mode as described in Sec. 3.3 to improve the peak-to-background ratio. In conventional measurements performed on the dual-detector setup, counts from both detectors were summed up in order to improve the counting rate and conventional S and W parameters were used in determining the shape of the annihilation line [94]. Also on the slow positron beams, the sample temperature could be controlled with a closed-cycle He cryostat and resistive heating.

It is also possible to measure positron lifetime in thin samples but for this a sophisticated pulsed positron lifetime beam is needed. In such a beam, the pulsing at a fixed frequency allows for the determination of the lifetime start signal even though the information of the original birth gamma is lost. More information on positron lifetime beams can be found in Ref. [100] and references therein.

4. The E center in silicon germanium

This chapter deals with the vacancy-group V donor pair, also known as the E center, in $Si_{1-x}Ge_x$. The thermal evolution of V-P pairs in proton irradiated $Si_{1-x}Ge_x$with Ge contents ranging from 10 to 30% is studied in Publ. I. A similar study but with varying dopant concentration instead of Ge content is performed on Sb-doped $Si_{0.8}Ge_{0.2}$ in Publ. II.

4.1 Thermal evolution of the V-P pair in n-$Si_{1-x}Ge_x$

Relaxed epitaxial $Si_{1-x}Ge_x$ layers ($x = 0.1, 0.2, 0.3$) *in situ* doped with $10^{18} P/cm^3$ and grown by chemical vapor deposition on Czochralski-grown Si(100) substrates as in Ref. [58] were measured with a slow positron beam. 2 MeV proton irradiation at a fluence of 1.6 $\times 10^{15}$ cm^{-2} was used to produce a homogenous defect distribution within the $Si_{1-x}Ge_x$ layer. The fluence was chosen high enough to produce saturated positron trapping into the generated V-P pairs.

In order to study the thermal evolution of these E centers, the samples were annealed in vacuum at five different temperatures ranging from 250°C up to 350°C. The total annealing times were 287 hours at 250°C, 76 hours at 275°C, 46 hours at 300°C and 4 hours at both 325 and 350°C and the annealing procedure

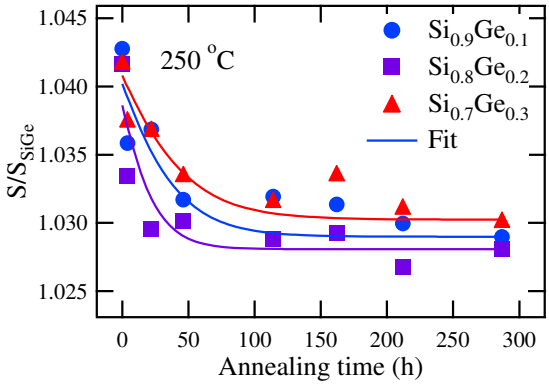

Figure 4.1. *Measured (markers) and fitted (lines) S parameters from $Si_{1-x}Ge_x$ annealed at 250°C. The starting points at 0 hours correspond to "as-irradiated" values associated with E centers.*

was identical for all samples. Positron Doppler broadening measurements were performed at room temperature between annealings and the obtained S and W values were normalized to the respective values (S_{SiGe}) of as-grown $Si_{1-x}Ge_x$ samples (e.g., the data from irradiated and annealed $Si_{0.9}Ge_{0.1}$ are scaled to untreated $Si_{0.9}Ge_{0.1}$ and so on).

In Fig. 4.1, the behavior of the S parameter as a function of time is shown for the sample annealed at 250°C. The annealing trend is similar for all the samples regardless of temperature; the S parameter stabilizes to a constant level (which still differs considerably from the as-grown sample) after an initial decrease. The decrease in S is an indication of the lattice recovering during the anneals but the fact that the parameter stays above the as-grown value means that the lattice never recovers to the state observed before the irradiation.

In order to get a better understanding of what happens to the E centers during the annealing, coincidence Doppler broadening measurements were performed on irradiated samples before and after annealing at 300°C. The results of these measurements are shown in Fig. 4.2. The data are normalized to the values from

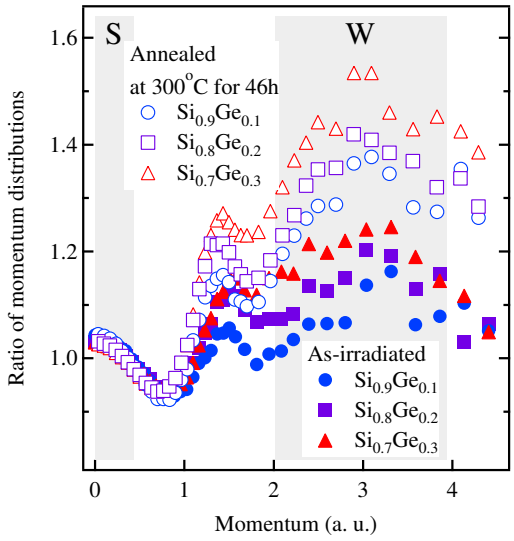

Figure 4.2. *Coincidence Doppler broadening results from irradiated* $Si_{1-x}Ge_x$ *before and after the annealing treatment.*

p-type silicon where no positron trapping into defects is observed. The intensity at high momenta is considerably higher than in the Si reference sample, indicating that there are Ge atoms around the annihilation sites. Prior to annealing, the average number of Ge atoms per vacancy depends on the Ge content in the sample and follows the expected statistics [56]. After the annealing, the Ge signal is much stronger in all samples which clearly indicates that the average number of Ge atoms is higher than after the irradiation.

The (S,W) plots of the longest annealed samples in Fig. 4.3 show that values obtained from $Si_{0.8}Ge_{0.2}$ and $Si_{0.7}Ge_{0.3}$ fall roughly on the line drawn between the initial state after the irradiation and the as-grown state. The points from $Si_{0.9}Ge_{0.1}$ however, are clearly above the line which suggests that the Ge decoration of the annealing sites is higher than the "random" Ge content would imply after annealing. This, in combination with the observations from the coincidence

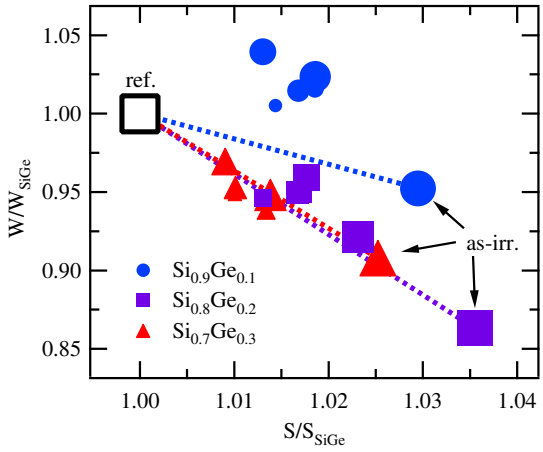

Figure 4.3. *(S,W) parameters of irradiated and annealed $Si_{1-x}Ge_x$ layers with varying Ge contents. The data shown are the final points of each annealing series. Decreasing symbol size visualizes an increase in annealing temperature. Values from each sample are scaled to the respective bulk*

measurements, leads us to conclude that high-order V-P-Ge$_n$ complexes with $n \geq 2$ are formed during the annealing regardless of Ge content provided the content is high enough. The formation threshold for these complexes seems to lie somewhere between 4 and 10% since they were not observed in Ref. [58]. The V-P-Ge$_n$ complexes eventually disappear over the course of the annealing, leaving behind Ge-rich clusters which explain the difference between the end states after the annealing and the as-grown state. Even though a positron has no preference to Ge core electrons compared to those of Si, the larger size of the Ge atom makes delocalized positrons overlap more with its electron cloud, thus making annihilations with Ge electrons more probable. This makes it possible to see the Ge clustering even without the presence of any positron traps.

A first order kinetic model was used to determine the annealing kinetics of the defects. Activation energies E_A of 1.5(2) eV for $Si_{0.9}Ge_{0.1}$, 1.3(2) eV for $Si_{0.8}Ge_{0.2}$ and 1.3(2) eV for $Si_{0.7}Ge_{0.3}$were obtained from Arrhenius plots drawn according

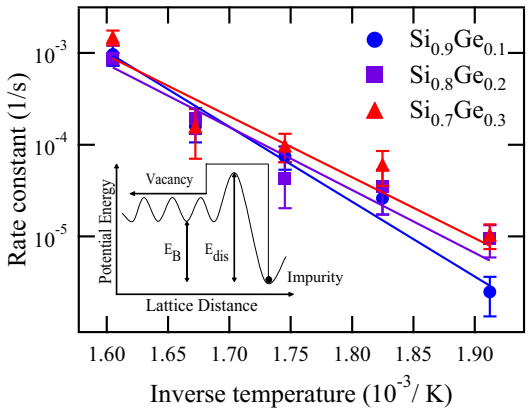

Figure 4.4. *Arrhenius plot for the annealing rate constant. The slope of the lines fitted to the experimental data points is interpreted as the dissociation energy for the diffusion of the E center in $Si_{1-x}Ge_x$. The insert shows a schematic representation of the dissociation (E_{dis}) and binding (E_B) energies of the vacancy-impurity pair.*

to the model (shown in Fig. 4.4). These activation energies are attributed to the dissociation of the vacancy-impurity complexes. The larger dissociation energy in $Si_{0.9}Ge_{0.1}$ reflects the behavior seen in Fig. 4.3. Both can be explained with the immediate vicinity of the defect being more different from the surrounding lattice in $Si_{0.9}Ge_{0.1}$ than in $Si_{0.8}Ge_{0.2}$ or $Si_{0.7}Ge_{0.3}$. The binding energy of the V-P pair was calculated to be 1.0(2) eV in $Si_{0.75}Ge_{0.25}$ by Chroneos *et al.* [101]. This value is in agreement with our result as it does not take into account the potential barrier shown in the insert of Fig. 4.4.

4.2 V-Sb pair in $Si_{0.8}Ge_{0.2}$

Relaxed 4 μm $Si_{0.8}Ge_{0.2}$ layers doped with 2×10^{18} and 2×10^{19} Sb/cm^3 were measured with positron Doppler broadening spectroscopy. The layers were grown

on p-type Si(001) substrates using molecular beam epitaxy. A graded SiGe buffer was included between the substrate and the $Si_{0.8}Ge_{0.2}$ top layer in which the Ge concentration was increased from 0 to 20% at a rate of 10% per micrometer. The samples were irradiated with 1.8 MeV protons in order to create a homogenous defect distribution within the $Si_{0.8}Ge_{0.2}$ layer. The proton fluence (10^{15} cm^{-2}) used in the irradiation was high enough to produce saturated positron trapping, i.e. a defect concentration $\gtrsim 10^{18}$ cm^{-3}, and the defects were identified as V-Sb pairs (E centers) [58].

The evolution of the E centers was studied by annealing the samples both isochronally and isothermally. In the isochronal annealing, the temperature was ramped up in steps of 50 K, starting from 350 K, and the sample was kept at each temperature for 30 minutes. The positron parameters were measured following each step at room temperature. The final temperature for isochronal annealing was 800 K. Isothermal annealings were done at two temperatures; 450 and 600 K. The annealing time steps were 60 minutes at 450 K and 30 minutes at 600 K. Also in this case, positron parameters were measured between annealing steps.

The S and W parameter evolution during the isochronal annealing is shown as a function of annealing temperature in Fig. 4.5. The defects start to anneal at around 400 K and the annealing is slow until 600 K. Between 600 and 650 K there is a very sharp drop in the S parameter indicating rapid annealing of the defects. After this drop, the samples seem to reach a stable state. Interestingly, this stable state – especially in the case of the W parameter (see Publ. II) – clearly differs from that obtained from as-grown material.

The (S,W) parameters from the isochronal experiment shown in Fig. 4.6 also reveal the clear difference between the stable state reached after annealing and the as-grown state. Since the difference is mainly in the W direction, a change in the chemical surroundings of the annihilation site is a likely explanation. An elevated W parameter such as the one in the sample with an Sb concentration of

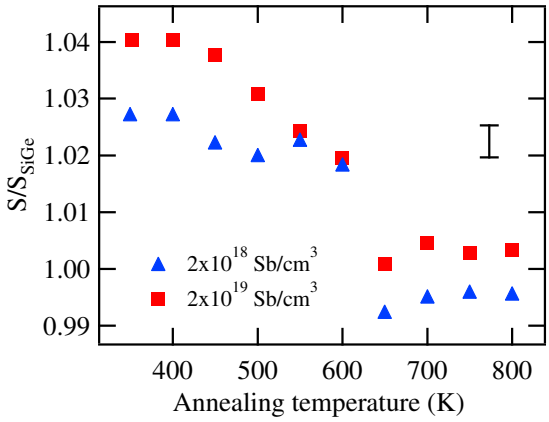

Figure 4.5. *S parameter as a function of annealing temperature in samples isochronally annealed at 30 minute steps. The values are scaled to those of as-grown* $Si_{0.8}Ge_{0.2}$. *The typical error margin of the parameters is also included.*

2×10^{18} cm^{-3} is characteristic for increased Ge decoration of the defects. In the other sample, however, the W value is actually lower than that of the as-grown sample, indicating that Sb also plays a role in the lattice evolution.

The isothermal experiment showed similar behavior to the isochronal one, with the exception of both samples expressing higher W parameters to those of the as-grown state after the annealing. This difference can be explained by more positrons annihilating with Ge core (3d) electrons. The Ge decorated E centers become unstable at high temperatures. Thus, the amount of these E centers was higher in the isothermal experiment as it was performed at lower temperatures than the isochronal one.

In Fig. 4.7, coincidence Doppler broadening results are shown for as-grown and annealed samples along with theoretical calculations for V-Sb and V-Sb_2 complexes in silicon [102]. The effect of Ge decoration is clearly seen in the high momentum region. The fact that the isochronal annealing has almost no effect in this region in the sample with a lower amount of Sb and a large effect in the other

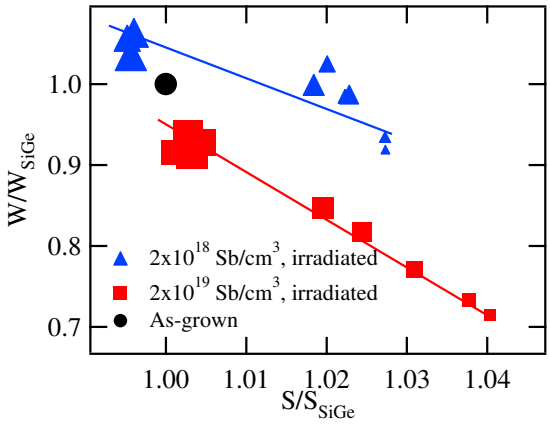

Figure 4.6. *S,W parameters measured in $Si_{0.8}Ge_{0.2}$ samples isochronally annealed at 30 minute steps. Increasing symbol size emphasizes increasing annealing temperature. The values have been scaled to those of as-grown $Si_{0.8}Ge_{0.2}$.*

one suggests that Sb acts as a stabilizing agent for the E centers and prevents them from finding Ge-rich areas in the sample. Another interesting feature is in the low momentum part of the spectra from isochronally annealed samples; it is very similar to the one from bulk Si, suggesting that the sample is in fact defect-free after the annealing even though there are differences in the W parameter. This is an indication of Ge clustering during the annealing – a phenomenon also observed in Publ. I.

4.3 E center evolution - a comparison between Si and $Si_{1-x}Ge_x$

As a conclusion to this chapter, it is natural to wrap up the recent results from phosphorus- and antimony-doped $Si_{1-x}Ge_x$ with previous experiments done on silicon [47]. In Fig. 4.8, schematics of E center evolution during isochronal annealing of both Si and $Si_{1-x}Ge_x$ are shown for P- and Sb-doped materials. The

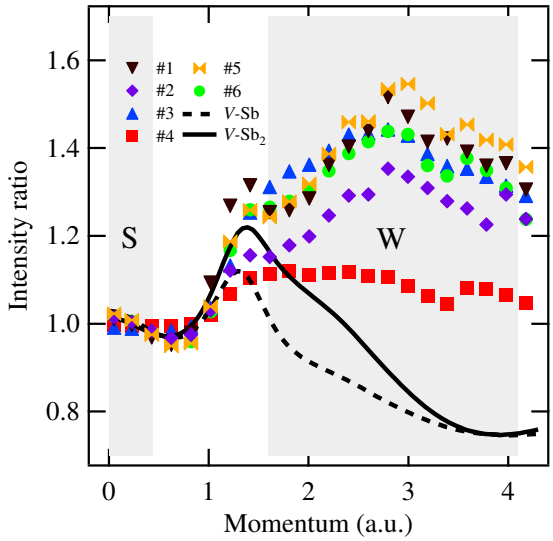

Figure 4.7. *Coincidence Doppler broadening results from $Si_{0.8}Ge_{0.2}$ samples along with theoretical calculations for V-Sb and V-Sb_2 defects in Si. All values have been scaled to those from bulk silicon. Samples 1 and 2 are as-irradiated ones with 2×10^{18} Sb/cm^{-3} and 2×10^{19} Sb/cm^{-3}, respectively. Samples 3 and 4 are the same annealed isochronally at 800 K. Samples 5 and 6 have been isothermally annealed for 3 hours at 550 K.*

effects of each change of defect type on the positron parameters are also shown.

Silicon is the easier case of the two materials since the only possible change regarding the E center is increased dopant atom decoration. In the case of P-doping, the E center can accumulate up to two additional P atoms around it. Each additional P atom lowers the positron S parameter slightly whereas W stays more or less constant. In the case of Sb only the change from V-Sb into V-Sb_2 was observed with positrons. This occurs above 600 K and is seen mainly as a considerable increase in W with S decreasing slightly. The third possible group V dopant in Si – As – behaves analogously to P. Si:As is not discussed here since in $Si_{1-x}Ge_x$ it is impossible to distinguish between As and Ge atoms with

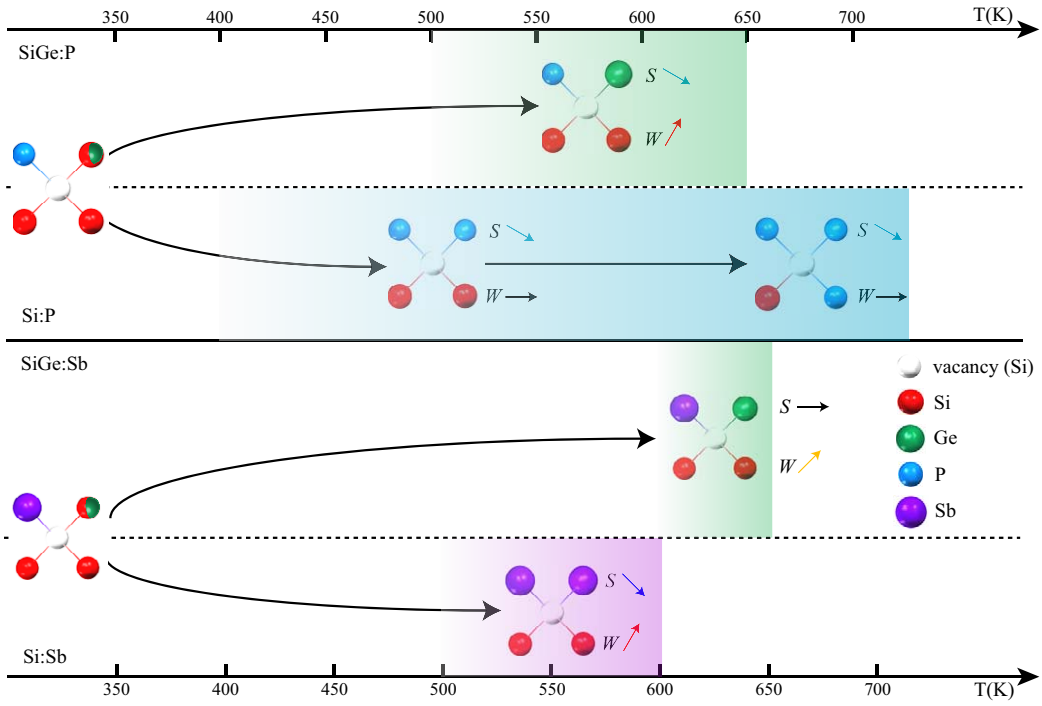

Figure 4.8. *Evolution of E centers in P- and Sb-doped Si and* $Si_{1-x}Ge_x$ *as a function of temperature in isochronal anneals. The highlighted areas show the temperature ranges for observing the defects shown within each highlight. Alongside each defect illustration, the evolution of positron parameters compared to the previous step in the process is shown with arrows. The half-red, half-green atom in the initial states indicates that in* $Si_{0.8}Ge_{0.2}$ *roughly half of the E centers have at least one Ge atom as a nearest neighbor*

coincidence Doppler broadening measurements due to the two elements having similar core electron structures.

In $Si_{1-x}Ge_x$:P, the situation is slightly more complex due to Ge atoms being also present in the lattice in addition to the dopants. The signature from Ge $3d$ electrons, though, is very strong when probed with positrons and thus it is

relatively easy to distinguish it from that of the dopant atoms. More or less all changes seen are due to Ge since P is very similar to Si with both having a $2p$ outer shell. The accumulation of Ge increases W and slightly lowers S. Ge decoration is quite slow in $Si_{1-x}Ge_x$:P and complexes with more than one Ge atom could only be seen after lengthy isothermal anneals.

$Si_{1-x}Ge_x$:Sb is the most complicated case presented here as both Ge and Sb have very strong characteristic annihilation signatures. The effect of additional Ge is similar to $Si_{1-x}Ge_x$:P and also here Ge decoration of more than one atom is only seen after long isothermal anneals. There is one major difference though as the effect of additional Ge atoms is not constant like in $Si_{1-x}Ge_x$:P as the second one affects the positron parameters more. Sb atoms have a similar effect to the parameters as Ge does but at a smaller magnitude. This can be explained by looking at Fig. 4.7; only a part of the Sb peak falls within the typical W window whereas the Ge effect contributes to W in its entirety. In our measurements, additional Sb atoms could not be observed around the E centers but they were regardless found to have an effect in the lattice evolution as shown in Publ. II.

5. Ion implantation- and irradiation-induced defects in germanium and silicon

In this chapter, defects introduced by radiation damage are studied in germanium and silicon. Proton irradiation at low temperatures and subsequent annealing is used to investigate simple vacancies in Ge in Publ. III. The effect of He-implantation in suppressing unwanted B diffusion in crystalline Si is studied in Publ. IV.

5.1 Vacancies in Ge after proton irradiation at low temperatures and subsequent annealing

In situ positron lifetime measurements were performed on weakly n-type doped ([Sb] $\approx 2\times10^{14}$ cm^{-3}) germanium after low temperature proton irradiation. The irradiation was performed with 9-10 MeV protons with a projected range of $\sim$400 μm in Ge and the proton fluence was varied from 1×10^{12} cm^{-2} up to 3×10^{14} cm^{-2} in order to be able to monitor the defect production. A fluence of $\sim1\times10^{14}$ cm^{-2} was needed to see a detectable increase in the average positron lifetime which is an indication of the presence of vacancies in the sample. A 10 MeV proton fluence of this magnitude typically generates 200-800 primary defects per centimeter in a semiconductor [99] which translates into a vacancy concentration of the order of

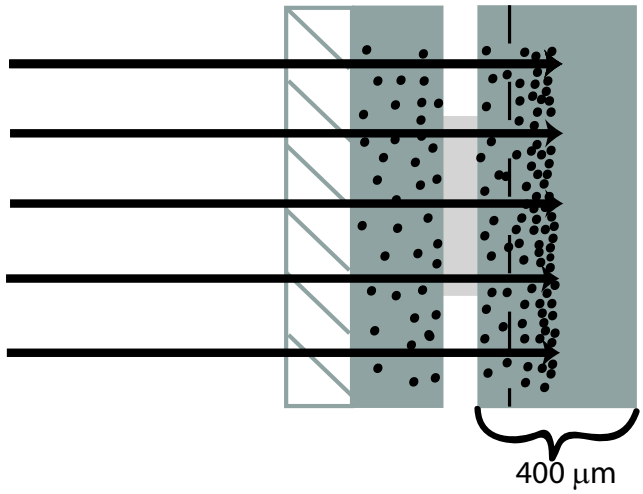

Figure 5.1. *Schematic of the sample sandwich used in the measurements. The positron source was placed between two sample pieces, one of which was ground to ∼250 µm. The grinding was done to avoid positrons from reaching the end-of-range voids in the inner sample piece. The irradiation damage is shown with black dots and the dashed line is drawn to visualize the mean implantation depth of the positrons*

10^{16} cm^{-3}. Most of the irradiations were performed at 35 K but some were done at 100 K in order to be able to distinguish between different annealing stages.

The samples were mounted in a standard sandwich setup [94], with a 20 μCi ^{22}Na positron source in between the two sample pieces. The outer sample piece was mechanically ground to a thickness of ∼250 μm (see Fig. 5.1) in order to get a homogeneous defect distribution within the positron implantation profile. By doing this, it was possible to make the positrons avoid seeing the end-of-range damage since the projected range of protons in Ge was around 150 μm into the inner sample and the mean positron implantation depth in Ge is only 80 μm.

The measurements were performed with a digital fast-fast positron lifetime spec-

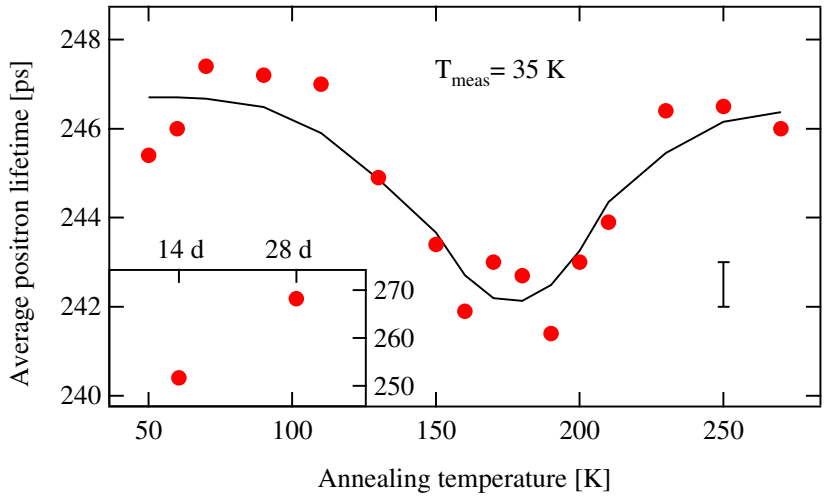

Figure 5.2. *Average positron lifetime as a function of annealing temperature in Ge after proton irradiation at 35 K. The insert shows the average lifetimes at room temperature after 14 and 28 days. All measurements except the ones in the insert were done at 35 K.*

trometer with a resolution of 260 ps. All measurements were done at 35 K with 30 minute annealing steps in the temperature range 35-300 K in between. Prior to measurements, the samples were allowed to cool down for approximately 4 days in order to avoid unwanted background from the decay of some radioactive As isotopes produced during the irradiation process.

In Fig. 5.2, the behavior of the average positron lifetime is shown during the course of the annealing after proton irradiation at 35 K. The average lifetime τ_{ave} is approximately 245 ps directly after the irradiation and thus well above the bulk value of 228 ps. Two distinct annealing steps can be seen in the figure: the first one a drop of ∼6 ps in the temperature interval 110-160 K and the second a similar increase in the interval 200-230 K. A spectral decomposition was not possible until after the first annealing stage, indicating that there are more than

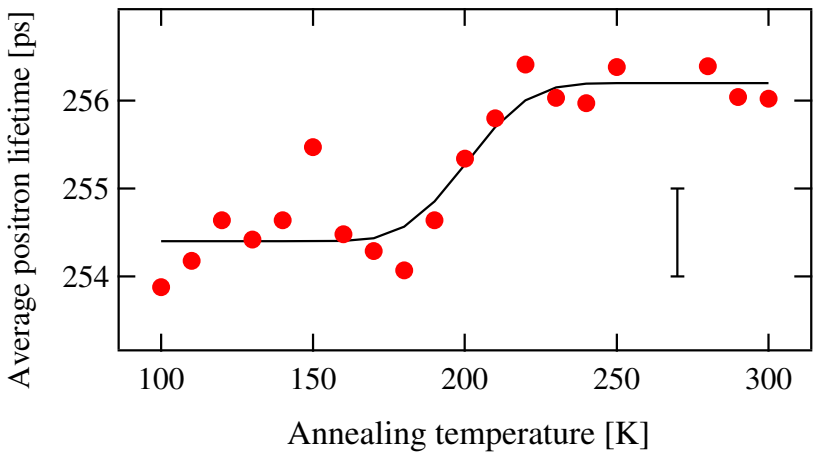

Figure 5.3. *Average positron lifetime as a function of annealing temperature in Ge after proton irradiation at 100 K. All measurements were performed at 35 K.*

one type of defects present in the sample following the irradiation. A successful two component decomposition could be performed from ∼200 K upwards but the defect lifetime component was evolving all the way up to room temperature, making an unambiguous identification of the defect species impossible.

Since the annealing was still continuing at RT, we decided to measure the sample a couple of times in atmospheric conditions after taking it out of the cryocooler. After 14 days, the average lifetime had risen to 252 ps and after 28 days it had finally stabilized at 268 ps. At that time, a successful decomposition of the spectrum according to the standard trapping model [94] was possible and a defect lifetime τ_2 of 315 ps was obtained.

In order to make the decomposition of the positron lifetime spectrum possible during the whole course of annealing and thus to be able to identify the positron traps, another proton irradiation was performed at 100 K. The measurement procedure was the same as for the sample irradiated at 35 K and the results can

be found in Fig. 5.3. As expected, the first annealing stage is now absent and τ_{ave} stays more or less constant up to 200K where a slight increase is seen. The decomposition of the spectra was possible now and a defect lifetime component τ_2 of 272 ps was obtained prior this annealing stage. After that, a continuous increase in τ_2 was observed.

The first annealing stage seen in samples irradiated at 35 K was attributed to the annealing of the Frenkel pair. The annealing temperature of 100 K is slightly higher than the ∼70 K obtained from DLTS experiments by Mesli *et al*. [103] but this can be explained by the observation of the annealing kinetics being slower in our case due to the several magnitudes higher concentration range. The absence of this annealing stage from samples irradiated at 100 K further strengthens the interpretation of it being attributed to the Frenkel pairs since they should no longer be stable at irradiation temperatures higher than 80 K.

The second annealing stage at 200 K was present regardless of irradiation temperature and was attributed to the annealing of the pure monovacancy. This conclusion was made from the results of the 100 K irradiations. The obtained defect lifetime component of 272 ps is clearly related to a defect of monovacancy size [94] and since no impurities are present in high enough concentrations, a vacancy-impurity complex can be ruled out. The standard trapping model [94] was used to obtain a concentration of 1.3×10^{17} cm^{-3} for these monovacancies prior to their anneal.

The continuous increases of both the defect lifetime τ_2 and the average lifetime τ_{ave} after the second annealing stage show that not all the monovacancies are annealing out but a considerable amount of them is combining into divacancies. The calculated divacancy concentration after the 300 K annealing in Fig. 5.3 is roughly 4×10^{16} cm^{-3} which means that approximately 60% of the vacancies form divacancies. The obtained lifetime of 315 ps is slightly lower than the 330 ps from previous positron measurements [69]. The cause of this difference might be due

to a considerable fraction of the divacancies being negative in this study since the overall divacancy concentration is much lower.

5.2 Vacancy clusters in He-implanted silicon

A slow positron beam was used at room temperature to measure Czochralski-grown n-type Si (100) implanted with 80 keV helium ions (projected range $R_p \approx 600$ nm) at various fluences ranging from 5×10^{15} to 8×10^{16} cm^{-2}. In addition to He-implantation, some of the samples were co-implanted with 12 keV B ions ($R_p \approx 50$ nm) at 5×10^{14} cm^{-2}. All implantations were performed at room temperature with ion fluxes of ∼1–2 μA/cm^2. Three samples were measured as-implanted and the rest were subjected to rapid thermal annealing at 800°C for 10 minutes. The native oxide layer was etched off the sample surfaces with HF prior to the measurements as it has been shown to skew positron results close to the surface [58].

Figure 5.4 shows an example of the S parameter data from all the samples with a He fluence of 3×10^{16} cm^{-2} and from the annealed samples with a fluence of 8×10^{16} cm^{-2}. B co-implanted samples are also presented. The most prominent feature in all the annealed samples is the high peak at positron implantation energies of 6–10 keV. This peak corresponds to the large voids at the R_p of He caused by the implantation. The interesting feature, however, is the shoulder slightly to the left of the peak (circled area in Fig. 5.4), at approximately 3–5 keV (or an average positron stopping depth of ∼100–300 nm). This shoulder is an indication of change in the positron diffusion length which means that an annihilation state different from the surface and the end-of-range voids exists there. The S parameter value of 1.06 times the Si substrate at the shoulder suggests "nanovoid" defects that are at least slightly larger than divacancies ($S_{V_2} = 1.05 \times S_{\mathrm{bulk}}$ [104]).

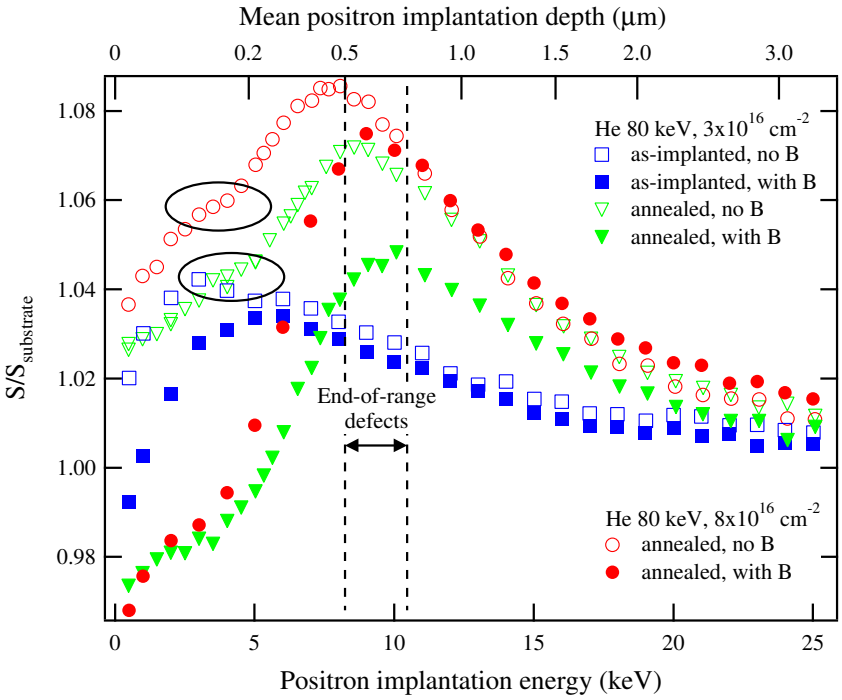

Figure 5.4. *The S parameter in the He-implanted samples with implantation fluences of* 3×10^{16} cm^{-2} *and* 8×10^{16} cm^{-2} *(only in annealed samples) as a function of positron implantation energy.*

The boron-implanted and annealed samples are clearly different from the ones without B. In these samples the peaks at R_p are smaller than in the samples with only He-implantation which means that either the end-of-range defects are smaller or their concentration is lower. The trapping in the nanovoid region at 3–5 keV is also different. The S parameter is close to the Si substrate value, suggesting that there are very few positron-trapping defects in the region. This is an indication of the nanovoids getting filled during the B-implantation. Since the diffusion length of B at 800°C for 10 min is only ∼140 nm in the case of interstitial supersaturation, the B atoms cannot reach the nanovoid region. Thus, the atoms

filling the nanovoids are self-interstitials created during the B-implantation. Previously obtained SIMS results, in which reduced diffusion of B has been observed at $R_p/2$, and transmission electron microscopy (TEM) results that suggest the presence of a nanovoid layer [73] are in good agreement with our results. The data from as-implanted samples both with and without B shows that the precursors of the nanovoids are already present and thus created during the He implantation.

Our results explain the mechanism in which He implantation creates approximately divacancy-sized defects at $R_p/2$ which then trap self-interstitials generated during the B-implantation. This leads to the reduction of B diffusion and creates a box-like B-implantation profile, making He co-implantation a useful tool for controlling B distribution in microelectronics applications.

6. Si nanoparticle interfaces in Si/SiO_2 solar cell materials

Interest in solar cells suitable for mainstream applications is growing all the time as fossilized fuels are gradually running out and the attitude towards nuclear power is trending towards negative among common people. In Publ. V, a novel solar cell material consisting of Si nanocrystals embedded within an SiO_2 matrix is studied with positron annihilation spectroscopy and photoluminescence.

Multilayer structures consisting of 30 Si/SiO_2 bilayers capped by an SiO_2 layer of 50 nm were deposited on *p*-type Si (100) substrates. The Si and SiO_2 targets were alternately sputtered in Ar gas at 3 mTorr. In the bilayers, the thickness of each SiO_2layer was 4 nm while Si layers of thicknesses of 1, 2 and 4 nm were employed in the three samples named as the 1 nm, 2 nm and 4 nm samples, respectively. Thus, the total thickness of the layer structure was either 200 nm, 230 nm or 290 nm. A pure SiO_2 layer of 300 nm used as a reference was also deposited on *p*-type Si substrate.

In order to form the Si nanocrystals, the samples were annealed in N_2 at 1100°C for one hour. Then each annealed sample was cut into two pieces and one of them was further annealed in 95% N_2 + 5% H_2 at 500°C for one hour in order to passivate defects [105–107]. Positron measurements were then performed on all three types of samples (as-deposited, once annealed and twice annealed). All

measurements were done with a slow positron beam in Doppler broadening mode at room temperature. Photoluminescence measurements were also performed on all samples. A continuous wave laser (Oxxius Violet) with a wavelength of 405 nm and excitation power of 50 mW was used as the excitation source. The PL spectra were measured at room temperature using a single monochromator (dispersion 0.8 nm/mm, resolution 0.008 nm) and a silicon photodiode. All spectra were corrected for the spectral response of the detection system.

The positron measurements revealed two trap states within the annealed samples. One of these states was attributed to the interface between the Si nanocrystals and the SiO_2 matrix and the other to the interface between SiO_2 and the Si substrate. Both states, along with the surface and the Si substrate states, are clearly visible in all samples as the results plotted on the (S, W) plane show in Fig. 6.1. The actual positions of both states in the figure are quite different between the samples with different Si layer thicknesses. Preliminary coincidence Doppler broadening results show that one of the interface states falling within the SiO_2 layer parameter range is purely coincidental; the signal at high electron momenta looks completely different between the two but the W parameter averages out to be roughly the same in both.

The signal from the (SiO_2/Si bulk) interface getting stronger as the Si layer thickness increases can be explained with the Makhovian implantation profile of slow positrons [109]. The profile is highly asymmetric and widens at high positron implantation energies. This means that in samples where the (SiO_2/Si bulk) interface is located deeper (i.e. the ones with thicker Si layers) and is probed with higher implantation energies, a larger fraction of the positrons reaches the interface and annihilates there.

The behavior of the other interface signal (2) is more interesting. This signal is the strongest in the 2 nm samples and considerably weaker in the other two. This correlates nicely with the photoluminescence results shown in Fig. 6.2. The PL

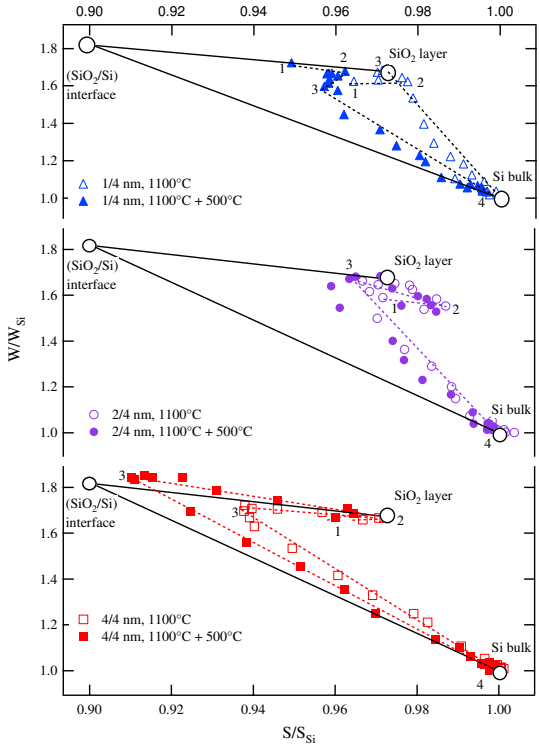

Figure 6.1. *Positron (S, W) parameters measured in annealed samples with three different Si layer thicknesses. The values are scaled to that of defect-free bulk Si. The bulk Si point, SiO_2 layer point and the (SiO_2/Si bulk) interface point from Ref. [108] are also shown. The four annihilation states: surface (1), first interface (2), second interface (3) and Si substrate (4) are marked for each sample. Both the solid lines connecting the three reference points and the dashed lines connecting the annihilation states are drawn to guide the eye.*

signal is by far the strongest in the 2 nm samples, distinguishable in the 4 nm samples and nonexistent in the 1 nm ones. The conclusion from this is that the nanocrystal formation is optimized in the 2 nm sample. Nanocrystals are formed also in the 4 nm sample but the weak signal by both techniques shows that the

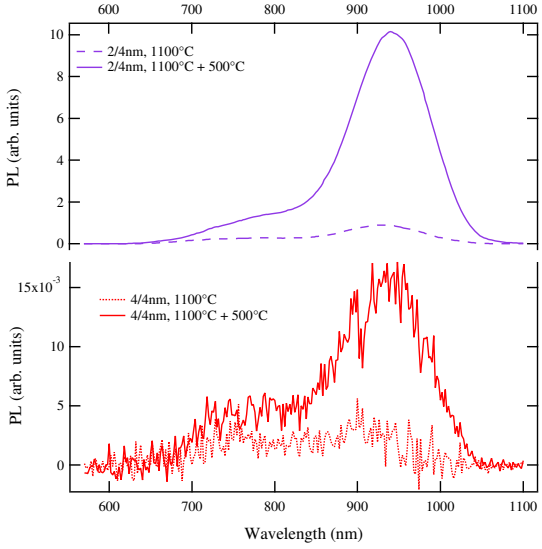

Figure 6.2. *Photoluminescence intensity as a function of wavelength for the samples with 2 (top panel) and 4 (bottom panel) nm Si layers. The 1 nm samples are not shown as they exhibit no PL at all.*

amount of active nanoparticles is lower. On a quick glance at Fig. 6.1 it would seem that the nanocrystal interface is seen by positrons also in the 1 nm sample but with a closer look it can be observed that this interface is different from the one seen in the 2 nm and 4 nm samples. This is best visible in Fig. 6.3 where the positron S parameters are plotted as a function of implantation energy for all three samples. The positron diffusion length changes considerably at $\sim$2 keV in the 2 nm and 4 nm samples whereas this region is almost flat in the 1 nm sample. Since there is no PL signal from the 1 nm sample, the likely explanation is that no nanocrystals are formed during the annealing in this sample but some other structural changes to which positrons are sensitive occur.

Results after the second annealing step at 500°C involving H are also presented

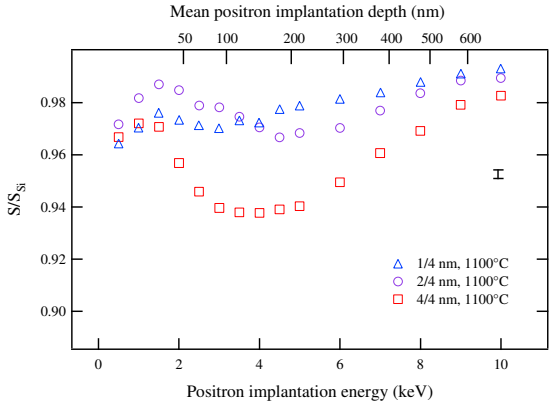

Figure 6.3. *S parameters as a function of positron implantation energy for samples with three different Si layer thicknesses annealed in N_2 at 1100° C . The values have been scaled to that of defect-free bulk Si.*

in Figs. 6.1 and 6.2. The increased PL intensity tells that H passivates the nanocrystal interfaces and thus makes the nanocrystals optically more active. This is also seen in the positron results as the S parameter at both interfacial states decreases in all samples. This indicates the reduction of free volume which is caused by H filling some of it. Thus, the annealing treatment for passivating the interfaces with H was found to be successful.

7. Summary

In this thesis, positron annihilation spectroscopy was used to investigate vacancy-type defects in two group IV semiconductors: Si and Ge, and their alloy $Si_{1-x}Ge_x$. Vacancies and other point defects typically form in semiconductor materials during growth and various processing steps. Point defects are usually detrimental to the electrical performance of the semiconductor since they are capable of creating new energy levels within the band gap, which then trap charge carriers. In many cases point defects also affect dopant diffusion and promote dopant clustering. Due to the latter these defects have become even more crucial for the semiconductor industry as the striving towards ever-smaller and more powerful devices requires both very shallow and very heavily doped regions in the semiconductor. Thus, a lot of effort has been put during the past decade towards understanding the basic nature of point defects such as their formation and how they can be removed efficiently without destroying the dopant profile in the process.

Positron measurements both in lifetime and Doppler broadening modes have been used to characterize vacancy-type defects at the atomic level. Publs. I and II deal with one of the most famous defects in group IV semiconductors – the vacancy-donor complex or the E center as it is often called. In Publ. I, the behavior of the V-P pair during isochronal annealing is studied in relaxed $Si_{1-x}Ge_x$with varying Ge contents. Ge decoration of the defects is observed during the course of

annealing and the random Ge distribution is found to no longer be valid after the treatment. Kinetics of the E center is also studied with the help of a first-order kinetic model. As a result, activation energies of approximately 1 eV are obtained for the dissociation of the V-P pairs. In Publ. II, the V-Sb pair is investigated in relaxed $Si_{0.8}Ge_{0.2}$ samples with varying doping levels. Both isochronal and isothermal annealing cycles are used in the experiments. The presence of Sb is found to stabilize the E centers during the annealing. Accumulation of Ge around the defects seen in Publ. I leading into Ge clustering is observed also in this study. In addition to presenting the results from Sb-doped $Si_{0.8}Ge_{0.2}$, an overview of different E centers and their behavior during isochronal annealing in both Si and $Si_{1-x}Ge_x$ is presented and discussed.

The vacancy in Germanium is studied in Publ. III with the help of low temperature proton irradiation followed by *in situ* positron lifetime measurements at 35 K. Two distinct annealing stages at 100 K and 200 K are observed. The first one is attributed to the Frenkel pair and the second to the monovacancy. A positron lifetime of 272 ps is obtained for the monovacancies. Divacancy formation is observed after the monovacancies become mobile and the divacancies are shown to be stable at room temperature, with a positron lifetime of $\sim$315 ps.

Beneficial effects of point defects are demonstrated in Publ. IV where divacancy-sized "nanovoids" created by He implantation are shown to successfully suppress interstitials created during B implantation of Si. The nanovoid layer is seen at approximately $R_p/2$ of He in He-implanted samples but is completely missing in samples co-implanted with B. Thus, interstitials created during the B implantation get trapped in the nanovoids. This confirms that He implantation is a helpful method when producing sharp implantation profiles of B in Si.

Finally, a novel solar cell material consisting of Si nanoparticles embedded within silica is studied with positron annihilation spectroscopy and photoluminescence in Publ. V. Si/SiO_2 multilayer structures with different Si layer thicknesses are

annealed at 1100°C in N_2 in order to form the nanocrystals. Samples with 2 nm thick Si layers are found to be optimal for nanocrystal formation by both techniques. Additional annealing at 500°C in 95% N_2 + 5% H_2 is performed in order to passivate defects. PL signal intensity is found to increase considerably following this anneal whereas a reduction in the positron S parameter is observed at the interface traps, indicating that H reaches the interfaces during the annealing.

Bibliography

[1] F. Schäffler, Semicond. Sci. Technol. **12**, 1515 (1997).

[2] J. Bardeen and W. H. Brattain, Phys. Rev. **74**, 230 (1948).

[3] S. Verdonckt-Vandebroek, E. F. Crabbe, B. S. Meyerson, D. L. Harame, P. J. Restle, J. M. C. Stork, and J. B. Johnson, IEEE Trans. Electron Devices **41**, 90 (1994).

[4] S. E. Thompson, M. Armstrong, C. Auth, S. Cea, R. Chau, G. Glass, T. Hoffman, J. Klaus, Z. Ma, B. Mcintyre, A. Murthy, B. Obradovic, L. Shifren, S. Sivakumar, S. Tyagi, T. Ghani, K. Mistry, M. Bohr, and Y. El-Mansy, IEEE Electron Device Lett. **25**, 191 (2004).

[5] M. L. Lee, E. A. Fitzgerald, M. T. Bulsara, M. T. Currie, and A. Lochtefeld, J. Appl. Phys. **97**, 011101 (2005).

[6] J. Bourgoin and M. Lannoo, *Point Defects in Semiconductors II. Experimental Aspects* (Springer-Verlag, Berlin Heidelberg, 1983).

[7] E. V. Monakhov, A. Y. Kuznetsov, and B. G. Svensson, Phys. Rev. B **63**, 245322 (2001).

[8] A. R. Peaker, V. P. Markevich, F. D. Auret, L. Dobaczewski, and N. Abrosimov, Journal of Physics: Condensed Matter **17**, S2293 (2005).

[9] S. Mirabella, E. Bruno, F. Priolo, D. De Salvador, E. Napolitani, A. V. Drigo, and A. Carnera, Appl. Phys. Lett. **83**, 680 (2003).

[10] L. Pelaz, M. Jaraiz, G. H. Gilmer, H.-J. Gossmann, C. S. Rafferty, D. J. Eaglesham, and J. M. Poate, Appl. Phys. Lett. **70**, 2285 (1997).

[11] H. Bracht, MRS Bull. **25**, 22 (2000).

[12] N. E. B. Cowern, A. J. Smith, B. Colombeau, R. Gwilliam, B. J. Sealy, and E. J. H. Collart, in *Proc. IEDM Technical Digest Electron Devices Meeting IEEE Int* (PUBLISHER, ADDRESS, 2005).

[13] A. J. Smith, N. E. B. Cowern, R. Gwilliam, B. J. Sealy, B. Colombeau, E. J. H. Collart, S. Gennaro, D. Giubertoni, M. Bersani, and M. Barozzi, Applied Physics Letters **88**, 082112 (2006).

[14] R. Gwilliam, N. Cowern, B. Colombeau, B. Sealy, and A. Smith, Nuclear Instruments and Methods in Physics Research Section B: Beam Interactions with Materials and Atoms **261**, 600 (2007), the Application of Accelerators in Research and Industry - Proceedings of the Nineteenth International Conference on The Application of Accelerators in Research and Industry, Nineteenth International Conference on The Application of Accelerators in Research and Industry.

[15] L. M. Fraas, Multilayer photovoltaic solar cell with semiconductor layer at shorting junction interface, 1981.

[16] R. R. King, D. C. Law, K. M. Edmondson, C. M. Fetzer, G. S. Kinsey, H. Yoon, R. A. Sherif, and N. H. Karam, Appl. Phys. Lett **90**, (2007).

[17] L. Tsakalakos, J. Balch, J. Fronheiser, B. A. Korevaar, O. Sulima, and J. Rand, Appl. Phys. Lett **91**, (2007).

[18] R. Krause-Rehberg and H. S. Leipner, *Positron Annihilation in Semiconductors* (Springer, New York, 1999).

[19] M. Lannoo and J. Bourgoin, *Point Defects in Semiconductors I. Theoretical Aspects* (Springer-Verlag, Berlin Heidelberg, 1981).

[20] S. Elliot, *The Physics and Chemistry of Solids* (Wiley, Chichester, 1998).

[21] H. Ibach and H. Lüth, *Solid-State Physics. An Introduction to Principles of Materials Science*, 3rd ed. (Springer-Verlag, Berlin Heidelberg, 2003).

[22] P. M. Fahey, P. Griffin, and J. D. Plummer, Rev. Mod. Phys. **61**, 289 (1989).

[23] E. E. Haller, Mater. Sci. Semicond. Process. **9**, 408 (2006).

[24] J. Vanhellemont and E. Simoen, J. Electrochem. Soc. **154**, H572 (2007).

[25] C. Claeys and E. Simoen, *Germanium-based Technologies* (Elsevier, ADDRESS, 2007).

[26] D. J. Paul, Adv. Mater. **11**, 191 (1999).

[27] T. E. Whall and H. C. Parker, J. Mater. Sci. - Mater. Electron. **6**, 249 (1995).

[28] R. Arghavani and H. M'saad, Solid State Technology **52**, 26 (2008).

[29] E. Kasper and D. J. Paul, *Silicon-Germanium Heterostructure Devices: Basics and Realisations* (Springer-Verlag, ADDRESS, 2005).

[30] Z.-Y. Cheng, M. T. Currie, C. W. Leitz, G. Taraschi, E. A. Fitzgerald, J. L. Hoyt, and D. A. Antoniadas, IEEE Electron Device Lett. **22**, 321 (2001).

[31] D. Chapin, C. Fuller, and G. Pearson, Journal of Applied Physics **25**, 676 (1954).

[32] D. Quick, Sunpower claims new solar cell efficiency record of 24.2 percent, 2010.

[33] A. Martí and M. Araújo, Solid State Technology **43**, 203 (1996).

[34] R. D. Schaller and V. I. Klimov, Phys. Rev. Lett. **92**, 186601 (2004).

[35] E. Cho, Y. Cho, T. Trupke, R. Corkish, and G. Conibeer, *Proc. 19th European Photovoltaic Solar Energy Conference, Paris* (PUBLISHER, ADDRESS, 2004).

[36] E. Cho, Y. Cho, J. Xia, R. Corkish, G. Conibeer, and Y. Huang, *Proc. 14th PVSEC Conf., Bangkok* (PUBLISHER, ADDRESS, 2004).

[37] G. Conibeer and et. al., Thin Solid Films **511**, 654 (2006).

[38] X. Hao and et.al., Thin Solid Films **517**, 5646 (2009).

[39] V. Osinniy, S. Lysgaard, V. Kolkovsky, V. Pankratov, and A. Nylandsted Larsen, Nanotechnology **20**, 195201 (2009).

[40] M. Zacharias, J. Heitmann, R. Scholz, U. Kahlere, M. Schmidt, and J. Blasing, Appl. Phys. Lett. **80**, 661 (2002).

[41] K. Surana, H. Lepage, D. Bellet, G. Le Carval, M. Baudrit, P. Thony, and P. Mur, *Photovoltaic Specialists Conference (PVSC), 35th IEEE* (PUBLISHER, ADDRESS, 2010).

[42] A. Nylandsted Larsen, A. Mesli, K. Bonde Nielsen, H. Kortegaard Nielsen, L. Dobaczewski, J. Adey, R. Jones, D. W. Palmer, P. R. Briddon, and S. Öberg, Phys. Rev. Lett. **97**, 106402 (2006).

[43] A. N. Larsen and A. Mesli, Physica B: Condensed Matter **401-402**, 85 (2007), proceedings of the 24th International Conference on Defects in Semiconductors.

[44] B. G. Svensson, B. Mohadjeri, A. Hallén, J. H. Svensson, and J. W. Corbett, Phys. Rev. B **43**, 2292 (1991).

[45] A. R. Peaker, V. P. Markevich, L. I. Murin, N. V. Abrosimov, and V. V. Litvinov, Mater. Sci. Eng., B **124-125**, 166 (2005).

[46] S. Hu, Phys. Rev. **180**, 773 (1969).

[47] V. Ranki, A. Pelli, and K. Saarinen, Phys. Rev. B **69**, 115205 (2004).

[48] L. C. Kimerling, in *Radiation Effects in Semiconductors*, Vol. 31 of *Institute of Physics Conference Series*, edited by N. B. Urli and J. W. Corbett (Institute of Physics, Bristol, 1977), p. 221.

[49] G. D. Watkins and J. W. Corbett, Phys. Rev. **134**, A1359 (1964).

[50] S. D. Brotherton and P. Bradley, J. Appl. Phys. **53**, 5720 (1982).

[51] J. Fage-Pedersen, A. Nylandsted Larsen, and A. Mesli, Phys. Rev. B **62**, 10116 (2000).

[52] C. E. Lindberg, J. L. Hansen, P. Bomholt, A. Mesli, K. B. Nielsen, A. N. Larsen, and L. Dobaczewski, Applied Physics Letters **87**, 172103 (2005).

[53] V. P. Markevich, A. R. Peaker, V. V. Litvinov, V. V. Emtsev, and L. I. Murin, Journal of Applied Physics **95**, 4078 (2004).

[54] E. V. Monakhov, A. Y. Kuznetsov, and B. G. Svensson, J. Appl. Phys. **87**, 4629 (2000).

[55] P. Kringhøj and A. Nylandsted Larsen, Phys. Rev. B **52**, 16333 (1995).

[56] M. Rummukainen, J. Slotte, K. Saarinen, H. H. Radamson, J. Hållstedt, and A. Y. Kuznetsov, Phys. Rev. B **73**, 165209 (2006).

[57] K. Kuitunen, F. Tuomisto, and J. Slotte, Phys. Rev. B **76**, 233202 (2007).

[58] S.-L. Sihto, J. Slotte, J. Lento, K. Saarinen, E. V. Monakhov, A. Y. Kuznetsov, and B. G. Svensson, Phys. Rev. B **68**, 115307 (2003).

[59] N. Cowern and C. Rafferty, MRS Bull. **25**, 39 (2000).

[60] S. C. Jain, W. Schoenmaker, R. Lindsay, P. A. Stolk, S. Decoutere, M. Willander, and H. E. Maes, J. Appl. Phys. **91**, 8919 (2002).

[61] M. D. Giles, Appl. Phys. Lett. **62**, 1940 (1993).

[62] M. D. Giles, J. Electrochem. Soc. **138**, 1160 (1991).

[63] P. Fahey, G. Barbuscia, M. Moslehi, and R. W. Dutton, Appl. Phys. Lett. **46**, 784 (1985).

[64] H.-J. Gossmann, T. E. Haynes, P. A. Stolk, D. C. Jacobson, G. H. Gilmer, J. M. Poate, H. S. Luftman, T. K. Mogi, and M. O. Thompson, Appl. Phys. Lett. **71**, 3862 (1997).

[65] H. Bracht and S. Brotzmann, Mater. Sci. Semicond. Process. **9**, 471 (2006).

[66] C. Janke, R. Jones, S. Öberg, and P. R. Briddon, Phys. Rev. B **75**, 195208 (2007).

[67] F. Poulin and J. Bourgoin, Rev. Phys. Appl. (Paris) **15**, 15 (1980).

[68] P. M. Mooney, F. Poulin, and J. C. Bourgoin, Phys. Rev. B **28**, 3372 (1983).

[69] K. Kuitunen, F. Tuomisto, J. Slotte, and I. Capan, Phys. Rev. B **78**, 033202 (2008).

[70] P. A. Stolk, H.-J. Gossmann, D. J. Eaglesham, D. C. Jacobson, C. S. Rafferty, G. H. Gilmer, M. Jaraíz, J. M. Poate, H. S. Luftman, and T. E. Haynes, J. Appl. Phys. **81**, 6031 (1997).

[71] D. De Salvador, E. Napolitani, G. Bisognin, A. Carnera, E. Bruno, S. Mirabella, G. Impellizzeri, and F. Priolo, Appl. Phys. Lett. **87**, 221902 (2005).

[72] E. Bruno, S. Mirabella, F. Priolo, K. Kuitunen, F. Tuomisto, J. Slotte, F. Giannazzo, C. Bongiorno, V. Raineri, and E. Napolitani, J. Vac. Sci. Technol., B **26**, 386 (2008).

[73] S. Mirabella, E. Bruno, F. Priolo, F. Giannazzo, C. Bongiorno, V. Raineri, E. Napolitani, and A. Carnera, Appl. Phys. Lett. **88**, 191910 (2006).

[74] E. Bruno, S. Mirabella, F. Priolo, E. Napolitani, C. Bongiorno, and V. Raineri, J. Appl. Phys. **101**, 023515 (2007).

[75] E. Bruno, S. Mirabella, E. Napolitani, F. Giannazzo, V. Raineri, and F. Priolo, Nucl. Instrum. Methods Phys. Res., Sect. B **257**, 181 (2007).

[76] C. C. Griffioen, J. H. Evans, P. C. De Jong, and A. van Veen, Nucl. Instrum. Methods Phys. Res., Sect. B **27**, 417 (1987).

[77] V. Raineri, M. Saggio, and E. Rimini, J. Mater. Res. **15**, 1449 (2000).

[78] V. Raineri and S. U. Campisano, Appl. Phys. Lett. **69**, 1783 (1996).

[79] V. Raineri, G. Fallica, and S. Libertino, J. Appl. Phys. **79**, 9012 (1996).

[80] D. K. Schroder, *Semiconductor material and device characterization*, 2nd ed. (John Wiley & Sons, Inc., New York, 1998).

[81] D. V. Lang, Journal of Applied Physics **45**, 3023 (1974).

[82] P. M. Mooney, in *Identification of Defects in Semiconductors*, edited by M. Stavola (Academic Press, San Diego, 1999), Vol. 51B, p. 93.

[83] L. Dobaczewski, A. R. Peaker, and K. B. Nielsen, Journal of Applied Physics **96**, 4689 (2004).

[84] S. Kasap and P. Capper, *Springer Handbook of Electronic and Photonic Materials* (Springer, ADDRESS, 2006).

[85] G. D. Watkins, Phys. Solid State **41**, 746 (1999).

[86] G. D. Watkins, Mater. Sci. Semicond. Process. **3**, 227 (2000).

[87] G. D. Watkins, in *Identification of Defects in Semiconductors*, edited by M. Stavola (Academic Press, San Diego, 1998), Vol. 51A, p. 1.

[88] M. Brustolon and G. Giacomo, *Electron paramagnetic resonance: a practitioner's toolkit* (John Wiley & Sons Ltd, ADDRESS, 2009).

[89] G. Pacchioni, L. Skuja, and D. Griscom, *Defects in SiO2 and related dielectrics: science and technology* (Springer, ADDRESS, 2000).

[90] D. B. Holt and B. G. Yacobi, *Extended defects in semiconductors* (Cambridge University Press, ADDRESS, 2007).

[91] S. Brotzmann and H. Bracht, J. Appl. Phys. **103**, 033508 (2008).

[92] H. Bracht, E. E. Haller, and R. Clark-Phelps, Phys. Rev. Lett. **81**, 393 (1998).

[93] H. Bracht, J. Fage-Pedersen, N. Zangenberg, A. Nylandsted Larsen, E. E. Haller, G. Lulli, and M. Posselt, Phys. Rev. Lett. **91**, 245502 (2003).

[94] K. Saarinen, P. Hautojärvi, and C. Corbel, in *Identification of Defects in Semiconductors*, edited by M. Stavola (Academic Press, San Diego, 1998), Vol. 51A, p. 209.

[95] P. Hautojärvi and C. Corbel, in *International School of Physics Enrico Fermi, Course CXXV*, edited by A. Dupasquier (IOS Press, Amsterdam, 1993).

[96] M. J. Puska and R. M. Nieminen, Rev. Mod. Phys. **66**, 841 (1994).

[97] P. Asoka-Kumar, M. Alatalo, V. J. Ghosh, A. C. Kruseman, B. Nielsen, and K. G. Lynn, Phys. Rev. Lett. **77**, 2097 (1996).

[98] I. Makkonen, M. Hakala, and M. J. Puska, Phys. Rev. B **73**, 035103 (2006).

[99] S. Vayrynen, P. Pusa, P. Sane, P. Tikkanen, J. Raisanen, K. Kuitunen, F. Tuomisto, J. Harkonen, I. Kassamakov, E. Tuominen, and E. Tuovinen, Nucl. Instrum. Methods Phys. Res., Sect. A **572**, 978 (2007).

[100] F. Reurings, Ph.D. thesis, Aalto University, 2010.

[101] A. Chroneos, H. Bracht, C. Jiang, B. P. Uberuaga, and R. W. Grimes, Phys. Rev. B **78**, 195201 (2008).

[102] M. Rummukainen, I. Makkonen, V. Ranki, M. J. Puska, K. Saarinen, and H.-J. L. Gossmann, Phys. Rev. Lett. **94**, 165501 (2005).

[103] A. Mesli, L. Dobaczewski, K. B. Nielsen, V. Kolkovsky, M. C. Petersen, and A. N. Larsen, Phys. Rev. B **78**, 165202 (2008).

[104] H. Kauppinen, C. Corbel, K. Skog, K. Saarinen, T. Laine, P. Hautojärvi, P. Desgardin, and E. Ntsoenzok, Phys. Rev. B **55**, 9598 (1997).

[105] A. R. Wilkinson and R. G. Elliman, Applied Physics Letters **83**, 5512 (2003).

[106] M. Yedji, J. Demarche, G. Terwagne, R. Delamare, D. Flandre, D. Barba, D. Koshel, and G. G. Ross, Journal of Applied Physics **109**, 084337 (2011).

[107] L. Koponen, L. O. Tunturivuori, M. J. Puska, and R. M. Nieminen, Phys. Rev. B **79**, 235332 (2009).

[108] H. Kauppinen, C. Corbel, L. Liszkay, T. Laine, J. Oila, K. Saarinen, P. Hautojärvi, M.-F. Barthe, and G. Blondiaux, J. Phys.: Condens. Matter **9**, 10595 (1997).

[109] P. Asoka-Kumar and K. G. Lynn, Appl. Phys. Lett **57**, 1634 (1990).

Aalto-DD 64/2011

ISBN 978-952-60-4229-9 (pdf)
ISBN 978-952-60-4228-2
ISSN-L 1799-4934
ISSN 1799-4942 (pdf)
ISSN 1799-4934

Aalto University
School of Science
Department of Applied Physics
www.aalto.fi

BUSINESS +
ECONOMY

ART +
DESIGN +
ARCHITECTURE

SCIENCE +
TECHNOLOGY

CROSSOVER

**DOCTORAL
DISSERTATIONS**